Use of Potential Flow Solvers for Automobile Racing Applications

by

Sajana Sathsara Ratnayake

A Thesis Presented in Partial Fulfillment
of the Requirements for the Degree
Master of Science

Approved November 2023 by the
Graduate Supervisory Committee:

Timothy Takahashi, Chair
Ruben Perez
Jeonglae Kim

ARIZONA STATE UNIVERSITY

December 2023

ABSTRACT

Formula 1 car front wings have evolved significantly over the last fifty years. Looking back at the past decade shows significant changes made due to rules and regulations by the Federation Internationale de l'Automobile and an increased understanding of aerodynamic concepts. There seems to be a trend where aerodynamic design concepts, previously seen in aviation, are being applied to Formula 1 front wings; this helps race teams increase downforce and reduce drag. This thesis analyzes these changes made over the past years and relates the material back to material that was learned by the aviation industry and attempts to synthesize conceptual Formula 1 front Wing designs using VORLAX, a vortex lattice panel method, used in the aviation industry. This insight would be beneficial for Formula 1 teams as there are budget and time restrictions applied to Computational Fluid Dynamic and wind tunnel testing, but panel methods are run in a matter of seconds as opposed to hours or days. So, if verified, preliminary designs can be rapidly tested to optimize the workflow and reduce the time required for Computational Fluid Dynamic and wind tunnel testing.

DEDICATION

This work is dedicated to my family. Thank you Heshani, my significant other, without whom I would have given up years ago. Thank you, mom, Gayani, for always having faith in me when making decisions. Thank you, sister, Sejini, for always having my back. And a special thanks to my late dad and late grandma, Jayantha and Rukmani, for empowering me to follow my dreams.

ACKNOWLEDGMENTS

As a student of ASU, I acknowledge that the Tempe campus sits on the ancestral homelands of those Native American tribes that have inhabited this place for centuries, including the Akimel O'odham (Pima) and Pee Posh (Maricopa) peoples.

I'd like to thank Dr. Timothy Takahashi for his guidance and mentoring over the past 5 years who provided me continuous support during my time as an ASU student. Thank you for pushing me through hard times and providing me with knowledge and advice for the future.

Thank you Dr. Jeonglae Kim and Dr. Ruben Perez for taking the time to be a committee member for my MS Thesis.

And last but not least, thank you to all faculty and staff at Academic and Student Affairs. Thank you for funding my education throughout my 2 master's degrees and for giving me invaluable knowledge and experience in becoming a better teacher.

TABLE OF CONTENTS

Page

LIST OF TABLES

Table Page

LIST OF FIGURES

Figure Page

CHAPTER 1

INTRODUCTION

Front and rear wing designs for Formula 1 cars have evolved significantly over the past fifty years. Significant improvements have been made, especially in the past two decades. More and more concepts used for aviation are applied to the pinnacle of the motorsport realm.

In aviation, there is the ability to use potential flow solvers such as VORLAX (Miranda, Elliott, & Baker, 1977) to run rapid synthesis simulations in order to predict airflow over the wing surfaces prior to running fully modelled computational fluid dynamic simulations which take significant resources to compute. This helps reduce the amount of time taken to synthesize aircraft wings significantly, especially when designing first iteration test wings. The question is, can panel method (i.e., vortex-lattice) potential flow software such as VORLAX be utilized in race car aerodynamic applications, specifically for front and rear wings, to similarly reduce the computation time needed for volume grid CFD simulations? And if so, how accurate are the results and what cautions need to be taken when doing so?

History of Formula 1 front Wings

Before diving into the technical material of aerodynamics, let us first check in on what type of front wings were used in Formula 1 cars over the decades.

Let us start 50 years ago, during the era of drivers like Niki Lauda and Gilles Villeneuve. In the 1970's, Formula 1 front wings had very simple front wings. The wings consisted of single-element front wings with one level of camber and twist and no geometry change throughout the entirety of the front. As seen in Figure 1, Formula 1 front wings did not start off as front wings separated from the car body in the early 1970's and protruded outwards directly from the nose of the car[1].

Figure 1: Formula 1 front Wings in the 1970s (Bersy, 2012)

[1] Disclaimer: The use of all external photographs in this thesis is from creative commons images from various websites. Please find the creative commons licensing information in the appendix. Additionally, there is no affiliation with any of the brands seen in such images.

Throughout the 1970s, note how developments to the front wings take place with the front wing having endplates added to keep the flow attached for longer and the front wing protruding outwards from the nose to have less effect on the body of the car. One can also see the camber getting more aggressive towards the trailing edge of the front wing here and the shape of the front wing evolves slightly. See Figure 2 below which shows these changes compared to Figure 1.

Figure 2: Endplates Added and Camber Increased in the 1970s (emkanicepic, 2019)

Starting from the 1980s, notice that the cars now compromise of two-element front wings. Note how in Figure 3, one can observe that the engineers are still cautious on ensuring minimum effect from the front wings onto the tires of the car and the body of the car by maintaining low profile wings which end before extending onto the front of the tires.

Figure 3: Formula 1 front Wings in the 1980s (Netsyscom, 2016)

In the 1990s, there seems to have been a significant development in the front wings where varying twist can be observed in the front wings. As seen in Figure 4, the planform geometry of the front wing seems to have been developed to obtain more surface area and there seems to be some spanwise twist in the central area of the front wing where the front wing attaches to the nose of the car. Note how this is similar to how the fuselage and wing of an aircraft are fused where significant twist is observed to obtain smooth flow over the surface of airplanes.

Figure 4: Formula 1 front Wings in the 1990s (Wilson, 2017)

Come the 2000s, and the wings have yet more significant developments taken place. Now the geometry of the front wing now starts to look to the more popular front wings that many people are aware of. Even in the 2000s, the front wing is still limited to only two-elements but now there is significant twist and camber variations across the

span of the wing. There also seems to be significant development in the endplates where the shapes are no longer just rectangles but varying geometry to obtain less turbulence in the tips of the front wing. As seen in Figure 5, the planform of the front wing also seems to be varying to obtain more preferrable airflow over the wing and the span of the wings also seem to be increasing drastically as the size of the cars also increase.

Figure 5: Formula 1 front Wings in the 2000s (Ulv, 2019)

The 2010s brought very complex front wings as seen below in Figure 6. These complex designs brought competitive advantages to well-budgeted teams while teams will lesser budgets struggled to keep up. This is also the era where there was a significant Mercedes-Benz AMG dominance where other teams were left far behind the top 3 teams.

Figure 6: Formula 1 front Wings in the 2010s (Toby_Parsons, 2018)

As a result of the large gap starting to form between highly funded teams and the rest of the grid, a lot more restrictions were put into effect. This includes, but is not limited to:

- Budget caps
- Additional geometry restrictions
- Simulation time limits
- Wind tunnel time limits

This gave way to the current front wings seen today as shown in Figure 7. Notice how the planforms of the front wings are standardized by regulations and significantly less complex compared to the front wings seen in the 2010s (Figure 6). This was also the new generation of Formula 1 cars where there are significantly smoother edges on the entire Formula 1 car which helped in aerodynamics and made the car more futuristic.

Figure 7: Formula 1 front Wings in the 2020s (randomwinner, 2019)

As expected, this brought the grid closer together where teams throughout the grid were able to compete more and more with the top teams, even though a different dominance, this time from Red Bull Racing, emerged. This is primarily due to the reintroduction of ground effect after it was banned in the 1980s as a result of collisions caused due to porpoising. Porpoising was a significant challenge for the teams in the 2022 year and this proved to be a hard challenge to overcome for most teams.

Porpoising occurs when there is flow separation on the lower surface of the Formula 1 car due to the car getting too close to the ground which stalls the airflow on the lower surface of the car. This leads to the car getting less downforce and the car moves back up which reattaches the flow to the lower surface and the cycle continues which results in the cars moving like porpoises.

Coming back to the focus on front wings, ground effect also brought in challenges to the front wings of Formula 1 cars. Because most of the ground effect generated being from the lower surface of the chassis of the Formula 1 car, this now meant that the front wings need to provide a more laminar flow behind it, so the aerodynamics of the chassis are able to perform optimally. Not only that, but the front wing needed to provide more downforce as doing so will reduce the amount of porpoising of the car as the first point of the car to lose airflow on the lower surface was the rearmost areas, which end up bottoming out. So, an obvious solution was to make the car more front heavy, to a point where some teams requested that additional weights be allowed on the nose of the car. However, teams were forced to work more with aerodynamics to overcome the solution, making the front wing development even more important.

Formula 1 cars prior to the 1970s will not be studied for the obvious reason of cars in the 1950s and 1960s not having front wings as seen in Figure 8.

Figure 8: Formula 1 Car in the 1950s (Pexels, 2016)

CHAPTER 2

PRIOR ART

This section of the thesis goes over important information that is required to understand the limitations of fluid flow and prior work completed by other individuals throughout the history of aviation and racecar aerodynamics.

Flow Conditions

To better understand the conditions at which Formula 1 cars operate, this subsection explains the estimated window that Formula 1 cars operate in. Formula 1 cars have varying operating speeds which can range upwards of 200 mph (Mach 0.26) when travelling down a straight section of a track to as little as 50 mph (Mach 0.065) when taking some corners in Monza and Bahrain and as little as 44 mph in Abu Dhabi (motorsport.com, 2017).

These speeds are consistent with Reynolds Numbers referenced to the wing chord being around 100,000 to 500,000 as $Re = \frac{\rho u L}{\mu}$ and the wing elements have typical chord length ranging from 4 to 8 inches. This provides dynamic pressures between 5 lbf/ft^2 in the tightest corners to 100 lbf/ft^2 in the long straights as $q = \frac{\rho u^2}{2}$.

Textbooks such as Aerodynamics for Engineers (Bertin & Cummings, 2014), explain the fundamentals of potential flow for 2D and 3D flows which are vital to understanding potential flows for wing design. It is explained that inviscid aerodynamic flow can be modelled using the potential flow equation:

$$\nabla^2 \Phi = 0 \tag{1}$$

Where the potential functions Φ relates to subsonic shock-free flow in Cartesian coordinates as explained by Prandtl (Prandtl, 1936)

$$\frac{d^2\Phi}{dx^2}\,(1 - M_\infty^2) + \frac{d^2\Phi}{dy^2} + \frac{d^2\Phi}{dz^2} = 0 \tag{2}$$

Where the physical velocity of the flow is defined in component form as:

$$u = \frac{d\Phi}{dx}\,; v = \frac{d\Phi}{dy}; w = \frac{d\Phi}{dz} \tag{3}$$

and the total velocity as:

$$V = \sqrt{u^2 + v^2 + w^2} \tag{4}$$

while incompressible pressures are proportional to the density and the net velocity:

$$P = \frac{1}{2}\,\rho\,V^2 \tag{5}$$

Note, for this application (race car) the Mach numbers are low enough that the Prandtl-Glauert term ($1 - M_\infty^2$) does not deviate substantially from unity. At 50 mph (Mach 0.065) the "Prandtl-Glauert" term is 0.996; at 200 mph (Mach 0.26) the term is 0.932. Thus, the flow is essentially incompressible; and the flow outside of the boundary layer should be accurately modelled using the Potential Flow Equation as shown above.

For Formula 1 front wings, the local Reynolds Number can be calculated as explained by White & Xue (White & Xue, 2021)

$$Re_x = \frac{\rho U x}{\mu} \tag{6}$$

where Re_x *is the local Reynolds Number,* ρ *is density,* U *is velocity,* x *is length at point of interest and* μ *is viscocity.*

At 50 mph near sea-level the Unit Reynolds Number is ~465,000/ft. At 200 mph near sea level, the Unit Reynolds Number is ~1,850,000/ft. This means that 0.1-ft aft of a wing leading edge, the local Reynolds Number varies from 46,500 to 185,000; the boundary layer flow is laminar. However, 1-ft aft of a wing leading edge, the local Reynolds Number can rise to 1,850,000; there the boundary layer flow is turbulent.

Since $\frac{\delta}{x}$ is given as

$$\frac{\delta}{x} \approx \begin{cases} \frac{5.0}{Re_x^{1/2}} & for\ laminar \quad 10^3 < Re < \sim 10^6 \\ \frac{0.16}{Re_x^{1/7}} & for\ turbulent \quad 10^6 > Re \end{cases} \tag{7}$$

$\frac{\delta}{x}$ is 0.088 → 0.139 0.1-ft aft of the leading edge; δ is ~0.009 → 0.014-ft, very thin. $\frac{\delta}{x}$ is 0.020 1-ft aft of the leading edge; δ is ~0.020-ft, still very thin. So, the boundary layer is only a few millimeters thick. Thus, the physical shape of the wing and the inviscid (outside of the boundary layer) shape are almost identical.

Limiting Factors for Flow Separation

Thin Airfoil Theory explains that the pressures due to camber, twist and thickness can be superimposed to predict the overall flow that occurs as a combination of the three pressures. This is because Thin Airfoil Theory suggests that the pressures due to camber, twist and thickness are linearly independent of one another, which provides the possibility to predict airflow of complicated designs by utilizing superposition.

It is vital to ensure that flow remains attached to the Formula 1 aerodynamic surfaces in all conditions to ensure that the vehicle remains in good aerodynamic balance. This ensures that the car is always controllable and can provide consistent performance throughout the duration of a race. So, it is important to find the limiting factors when it comes to flow separation to ensure that the designs tested stay well below that limit. A. M. O. Smith (Smith, 1975) discusses the theoretical upper limit of lift in a potential flow field for a structure with circular camber where the stagnation points occur at the same point. While this provides an upper limit for lift coefficient as 4π, this is unrealistic for airfoils that are created for any aviation or racing applications.

Instead, one can calculate the maximum lift coefficient based on the lift equation:

$$C_L = \frac{2L}{\rho u^2 S_{ref}} \tag{8}$$

$where\ C_L = lift\ coefficient, L = Lift\ (or\ in\ our\ case, downforce), \rho = density\ of\ air$ and $S_{ref} = planform\ reference\ \ area.$

The next important limiting factor is stagnation, which occurs at the maximum positive pressure that can act upon a wing. We know that:

$$C_p = \frac{p - p_\infty}{q_\infty} = +1 \tag{9}$$

$where\ C_p = pressure\ coefficient, p = static\ pressure\ at\ given\ point$ $p_\infty = freestream\ static\ pressure$ and $q_\infty = freestream\ dynamic\ pressure.$

To have a satisfactory pressure distribution, the stagnation pressure location can be forced to occur closer to the leading edge and ensuring the remainder of the wing has pressure coefficients less than 1.

Mayer (Mayer, 1948), suggests that a practical limit of 70% vacuum for leeward and windward side pressures are a good practical limit which is given by:

$$C_p^* = \frac{p - p_\infty}{0.7 p_\infty M_\infty^2} \tag{10}$$

$where\ C_p^* = critical\ pressure, p = static\ pressure\ at\ given\ point\ p_\infty =$ $freestream\ static\ pressure$ and $M_\infty = freestream\ Mach\ number.$

Under isentropic conditions, this can be written as:

$$C_p^* = \frac{1}{0.7 M_\infty^2} \left[\left(\frac{1 + 0.2 M_\infty^2}{1 + 0.2 M^2} \right)^{3.5} - 1 \right] \tag{11}$$

An alternate method for calculating critical pressure is using Küchemann's critical pressure equation (Küchemann, 2012):

$$C_p^* = \frac{2}{\gamma M_\infty^2} \left\{ \left(\frac{2}{\gamma + 1} \right)^{\frac{\gamma}{\gamma - 1}} \left(1 + \frac{\gamma - 1}{2} M_\infty^2 (cos\phi)^2 \right)^{\frac{\gamma}{\gamma - 1}} - 1 \right\} \tag{12}$$

$where\ C_p^* = critical\ pressure, \gamma = specific\ weight,$

$M_\infty = freestream\ Mach\ number$ and $\phi = sweep\ angle.$

Plotting these equations for our region of interest gives us the Figure 9 below. For Formula 1 cars, this gives a limiting suction-side critical pressure of *Cp* ~ -12.

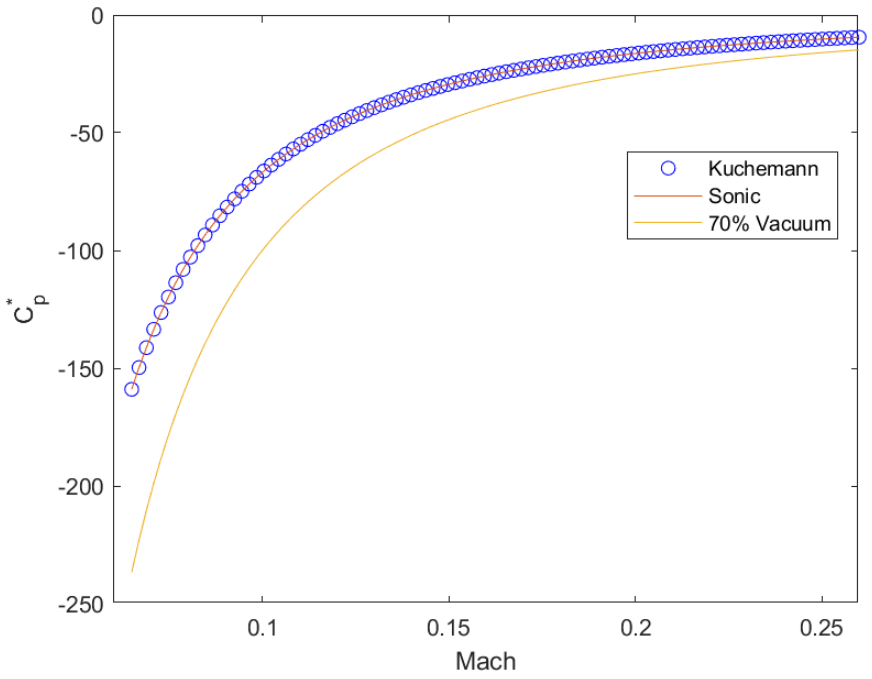

Figure 9: Critical Pressure vs Mach Number

When it comes to highly twisted airfoils, there comes a point where initially, as large amount of downforce is generated by and airfoil, but when twisted, more and more of the airfoil starts creating more drag than downforce, making further twisting of the wing less feasible. This can be visualized in Figure 10.

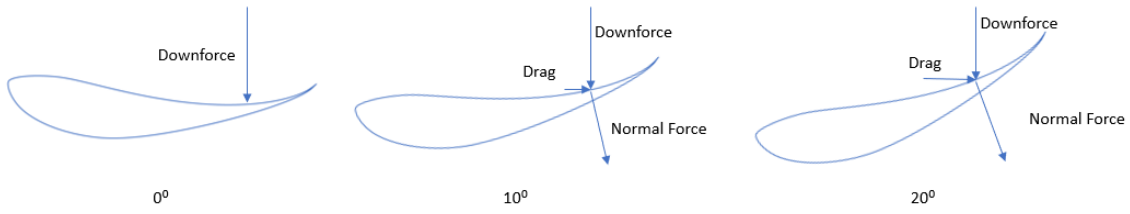

Figure 10: Drag Increases and Downforce Reduces as Incidence Increases

Similarly, if camber is increased past a certain point, the components contributing to drag increases and the components contributing to downforce reduces. This is because the local surface inclination of the airfoil is changed because of camber being increased. Figure 11 shows this using the S1210 airfoil below.

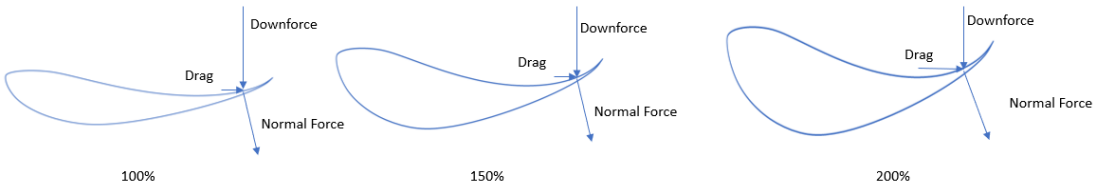

Figure 11: Drag Increases and Downforce Reduces as Percent Camber Increases

Racecar Aerodynamics

Katz explains the limitations of racecars due to lack of downforce very clearly in his 2006 paper (Katz, Aerodynamics of race cars, 2006). The increase of downforce in racecars lead to higher possible acceleration due to more grip being available when getting the car to accelerate and the car being able to corner at faster speeds due to more lateral grip being available when cornering, especially at high-speed corners. While higher quality tires can provide this required grip, the distribution of the downforce plays an important role as the stability of the racecar is heavily dependent on this weight distribution between the front and rear wheels. Using aerodynamic components such as the front and rear wings, and in recent years the car's body itself and underbody venturi tunnels, can help distribute this weight with more control. In fact, Katz explains that the

significant increase in performance for Formula 1 cars from the 1960s to the 1990s is due to the introduction of these aero surfaces where the cornering acceleration grew from under 1g (where g is the gravitational acceleration which is 9.81 m/s^2 or 32.17 ft/s^2) to 4g.

Katz also explains that race car lifting surfaces are different from airplane wings due to:

- race car front wings operating within strong ground effect,
- open-wheel race car rear wings having very small aspect ratio when compared to airplane wings, and
- strong interactions between the wings and other vehicle components such as the wheels and race car body.

Katz discusses further some important developments that came from understanding the flow conditions in race cars such as the reduction of drag by adding Gurney flaps which helped reduce the amount of drag created by race car wings (seen first in the Liebeck in 1978).

In Katz's book Automotive Aerodynamics (Katz, Automotive Aerodynamics, 2016), Katz discusses the various methods used for performing Computational Fluid Dynamics on cars. On page 331, Katz extensively describes the governing equations for fluid flow in panel methods, which is similar to Bertin & Cummings, 2014 and also discusses the pros and cons of using panel methods. Katz explains how panel methods are less computationally demanding resulting in very efficient methods but only apply to inviscid attached flows.

Superposition and Incorporating Panel Methods

In 2010 Donovan & Takahashi (Donovan & Takahashi, 2010) explored an algorithm using an unconstrained gradient based solver which optimizes conceptual wing designs for airplanes. This method used a root-mean-square function to minimize the error between a target spanwise lift distribution and the estimated transverse span load and varied the twist across the wing to achieve this.

Donovan & Takahashi reorganize the Korn equation to make thickness over chord length the subject of the equation to get:

$$\frac{t}{c} = K - .1 * C_l - M_{crit} \tag{13}$$

$where\ \left(\frac{t}{c}\right) is\ the\ local\ thickness, K\ is\ the\ technoloy\ factor,$

$C_l\ is\ the\ local\ section\ lift\ coefficient\ and\ M_{crit}\ is\ the\ critical\ Mach\ number$

The local lift coefficient was determined by:

$$C_l(y) = \frac{Lift(y)}{q * c(y)} \tag{14}$$

$where\ q\ is\ dynamic\ pressure, Lift\ is\ the\ design\ lift\ distribution\ and$

$c(y)\ is\ the\ defined\ geometry.$

Jensen & Takahashi (Jensen & Takahashi, 2016) take this a step further by analyzing the three-dimensionality of the flow when conducting superposition of camber, twist and thickness to achieve target lift. Jensen & Takahashi start by exploring the effects of different wing shapes, taper ratios and aspect ratios.

Recent Automotive Wing Design Publications

In 2020, Castro & Rana (Castro & Rana, 2020) published a paper on exploring the structure, materials, weight, and aerodynamics of Formula 1 front wings that affect overall aerodynamics performance of Formula 1 cars. Of the aerodynamics concepts explored in the research conducted by Castro & Rana, the most intriguing work was the exploring of the effects due to the introduction of multi-element front wings and the addition of endplates to the designs. Castro & Rana used ANSYS Fluent 2019 which is a finite volume method that solves the partial differential equations associated with fluid flow. More specifically, Castro & Rana use the Reynolds Averaged Navier-Stokes equations modeled by the k-ω SST turbulence model where they claim an optimal balance between accuracy and computation time for running the cases tested. The fluid dynamics model they used was a coupled incompressible solver based on the SIMPLE algorithm.

CHAPTER 3

METHOD

For most of the research presented below, VORLAX was used to conduct the simulations. VORLAX is a Vortex-Lattice Potential Flow solver developed by Luis Miranda in the 1970s (Miranda, Elliott, & Baker, 1977). Souders & Takahashi (Souders & Takahashi, 2021) improved the current version of VORLAX by decreasing the runtime of the solver, increasing the total number of points, correcting grid spacing issues, improving the solver initial guesses and adding multiple error messages for diagnostics. Research conducted by Souders & Takahashi allowed the new version of VORLAX to run more complicated wing designs than initially capable by the original solver.

For all cases that were tested in the research conducted for this thesis, sandwich panels were utilized to model the upper and lower surfaces of the aerodynamic bodies.

Previous Work on Panel Methods and Superposition

Prior to working on Formula 1 front wings for my research, I was conducting research on conceptual airplane wing design synthesis. In order to understand some of the aerodynamics explored later in this thesis, some of the material learned earlier about airplane wings and the insights gained from simulations done on airplane wings will be very helpful.

In 2021, I was able to publish a conference paper based on research that was completed to verify and improve the work done by Donovan & Takahashi in 2010 and Jensen & Takahashi in 2016. Using penalty functions and superposition principles, I was

able to explore more into developing algorithms that use principles of superposition to make synthesis of conceptual design wing lofts more straightforward. This research mostly came being due to the final project of the Advanced Aerodynamics course that Dr. Takahashi teaches at Arizona State University. During the final project, myself and my teammate, Bhargav Chaudhari, spent multiple days synthesizing wing designs required for the constraints given for the project. The constraints for our specific airplane (as each team's was unique) were:

- Design Critical Mach Number 0.78
- Design Altitude 35,000 ft
- Design Lift 110,000 lbm
- Wingspan (tip-to-tip) 100 ft
- Fuselage Length 115 ft
- Fuselage Diameter 11 ft
- Wing Fuselage Junction 45 ft

During this project, the main issue was whenever a spanwise lift distribution and pressure contour was analyzed for a designed wing, the smallest iteration of a control point along the wing led to the lift and pressure at other spanwise locations along the wing changing drastically as a perturbation at one control point affects the entire spanwise loading. In fact, multiple EXCEL sheets were generated even at this stage to automate the visualization of lift and pressure over the airplane wing.

As a result of this frustration, the research presented in my 2021 SciTech Forum paper was published as a conference paper. To mention the important findings concisely,

it was confirmed that as published by Donovan & Takahashi in 2010, twist can be superimposed to achieve target spanwise lift distributions while ensuring that the critical pressure, as calculated using Küchemann's equation, is not reached results in well performing conceptual wing lofts.

Similarly, adding on camber as a perturbation parameter also shows that the trends hold as expected for most scenarios. The caveat is that there seems to be some error between the expected and actual spanwise lift distributions when looking at higher multipliers for the twist and camber perturbations. This led to the additional research conducted by myself and Dr. Takahashi with results published in the 2022 SciTech conference.

The results discussed in this section relate to airplane wing synthesis with the following planform and control points seen in Figure 12. Note that for the context of this thesis, control points refer to the geometry design control point. For the research conducted on airplanes, seven control points were used so that there were sufficient control points to vary the twist, camber and thickness along the wing. Three of the control points were for the Yehudi and four of the control points were for the remainder of the wing.

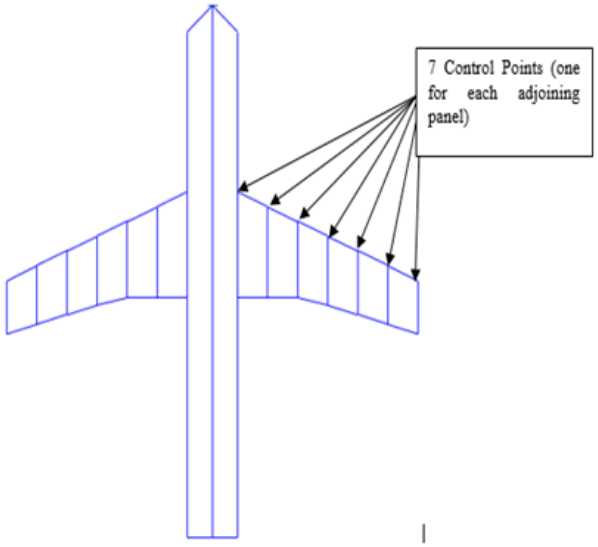

Figure 12: Geometry and Control Points for Airplane Wing Design

As seen in Figure 13, it was evident that perturbing twist at higher and higher multipliers did not seem to introduce a significant error to the value predicted. Note that even at the 15° perturbation point, extrapolating the 1° twist perturbation gave results that were comparable to the simulated 15° perturbation.

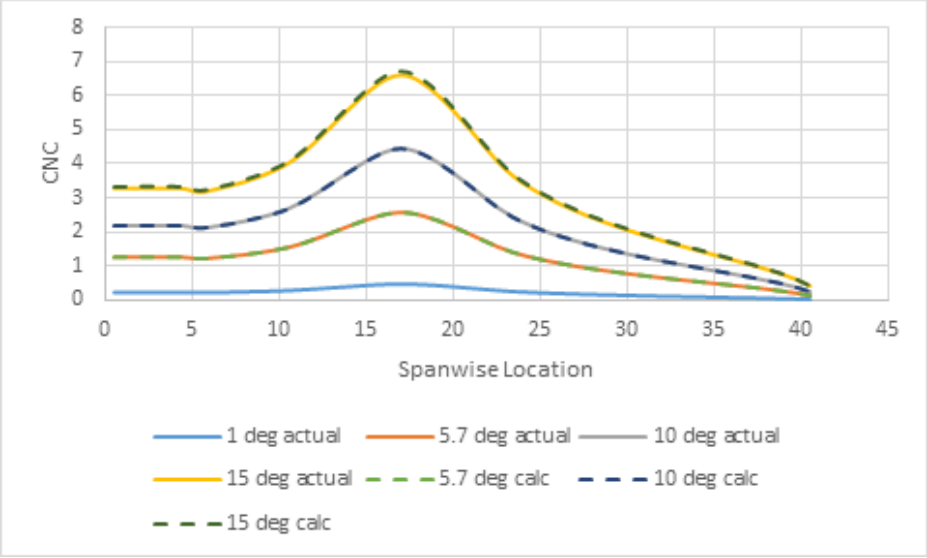

Figure 13: Twist Perturbation at Higher Values

The cause for concern was when camber was perturbed at higher multipliers as it became apparent that camber did not superimpose linearly as predicted. This is because the direction cosines change as the camber profile is multiplied to achieve a target spanwise lift distribution. This causes a change in the camber profile which leads to the simulated wing not having the same expected spanwise lift distribution as the calculated wing.

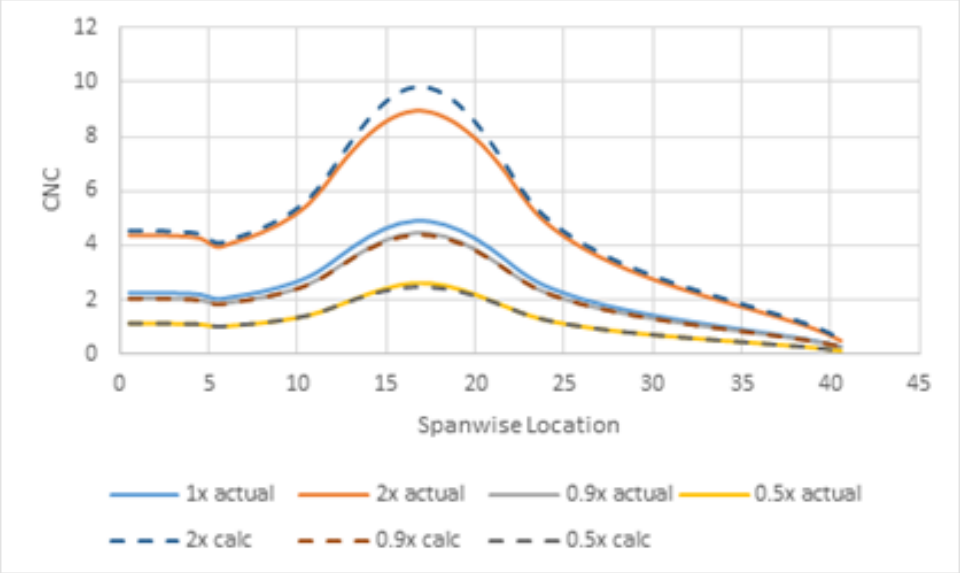

Figure 14: Camber Perturbations in Higher Values

Thickness should not play a significant role when it comes to spanwise lift distributions as their upper and lower panels are which leads to lift cancelling out. However, a verification was done as seen in Figure 15 to ensure that the effect of thickness on spanwise lift distributions was minimal. Unsurprisingly, this was verified as the lift generated by the thickness profile was negligible. And as seen in Figure 15, the little lift that was generated was multiplying linearly, similar to the twist case.

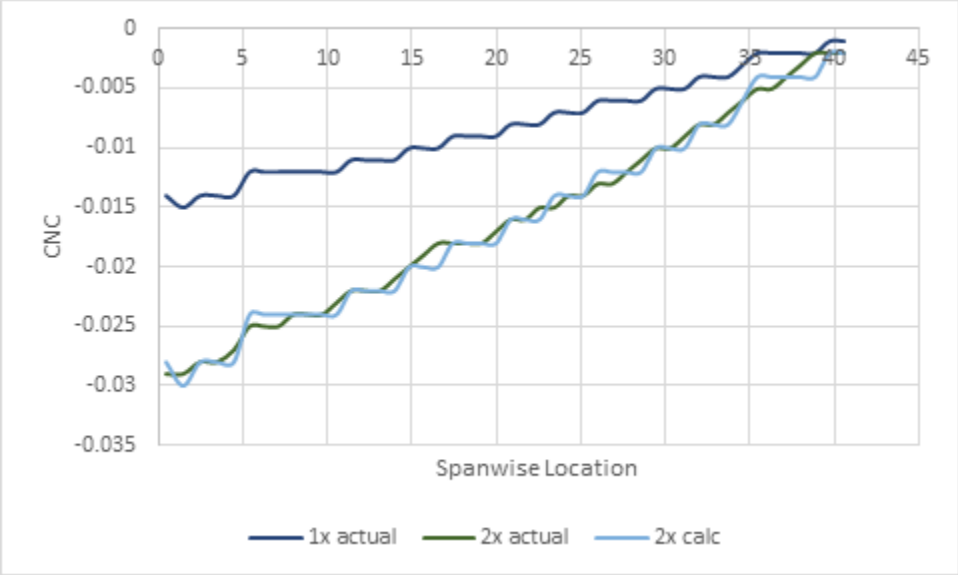

Figure 15: Thickness Perturbations in Higher Values

A way to overcome the issue with camber interpolation was to develop a 2-step approach. Camber, twist and thickness were perturbed (this is explained in more detail in the METHOD portion of this thesis), and a first run was completed to get approximate lift and pressure multiplier for each control point. Then, a 2nd step was carried out where the new perturbation were the expected multipliers from the 1st step multiplied by the initial profile at each control point. This provided a more realistic lift and pressure profile at each control point for the expected multipliers. A second synthesis was then done using the new twist, camber and thickness profiles obtained from the first step. This led to the predicted lift and pressure profiles being very similar to the lift and pressure profiles simulated for the obtained parameters.

If done correctly, the multipliers at the 2nd step need to be very close to 1. The values obtained for camber for a test scenario were 0.9574, 1.0882, 1.0761, 0.9369, 1.0882, 0.9516 and 1.0000 (to 4 decimal points). As it can be noted, these values are very

close to 1, but different enough to produce some deviation from the one-step method done in the research presented in 2021. This insight gained from airplane design proved to be useful for synthesis of Formula 1 front wings as well. Especially since the newer Formula 1 front wings have a significant amount of twist and camber applied to them.

Python as a Solver Algorithm

In order to automate the processes done for the simulations mentioned above, various Python scripts were written.

The first script was for the generation of the input files for obtaining the perturbation profiles for lift and pressure. Each control point was perturbed at the required twist, camber and thickness profiles and the cases were automatically run on VORLAX once the files were generated. The LOG files were then saved for each case and the user needs to scrape off the CNC (lift per spanwise location) and DCP (pressure at each location). There was an attempt to automate this scraping but this was not a success.

The scraped data was then input into *PyCharm* and an optimization algorithm was run based on achieving minimum error between a target spanwise lift distribution and a current spanwise lift distribution by varying the multipliers of twist, camber and thickness at each control point. While many methods were tested out for this, the best results were obtained using the *SciPy.optimize* function in the *SciPy* package. For the 2nd step, the same process was carried out once again but using newly generated input data obtained by multiplying the twist, camber and thickness profiles by the multipliers

obtained from the first step. This resulted in the lift and pressure contours seen in Figure 16 and Figure 17.

Figure 16: Spanwise Lift Distribution Obtained from two-step Algorithm

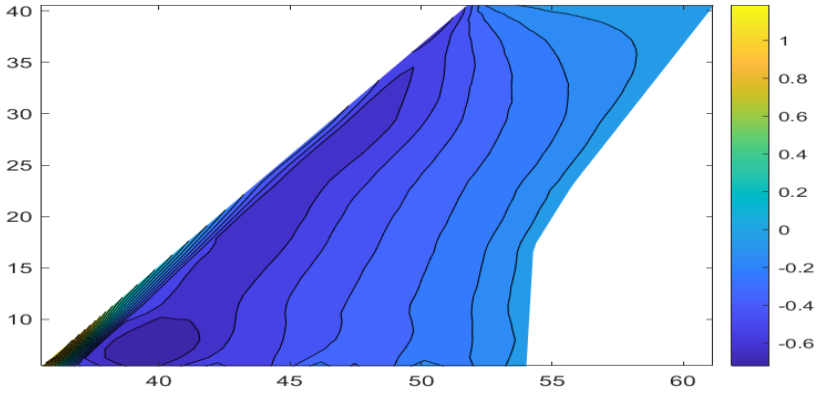

Figure 17: Pressure Contour Obtained from two-step Algorithm

Single Element Wing

The first step in the research conducted on Formula 1 front wings was to synthesize a feasible wing using only one panel. This represents the early Formula 1 front wings where a simple extrusion was used with no variation in camber, thickness, or twist throughout the span of the front wing. There is very little that can be done here to improve the wing design as only one camber profile and one value of twist can be used throughout the entirety of the single element.

So, for presenting the data for this research, only the case of 50% S1210 camber profile will be used. The trends observed for lift and drag coefficients when the angle of attack was varied can be seen in Figure 18 and Figure 19.

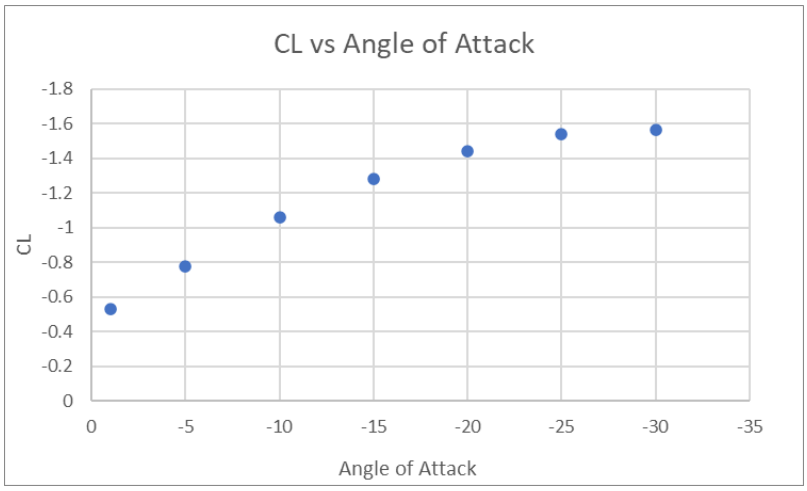

Figure 18: Coefficient of Lift vs Angle of Attack

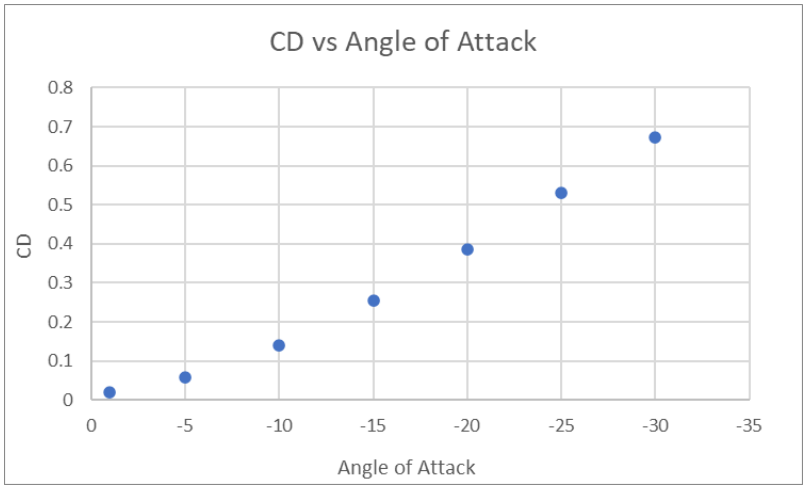

Figure 19: Coefficient of Drag vs Angle of Attack

As it can be seen in Figure 19, initially, the increase in angle of attack provides a significant increase in downforce, almost linear in nature. At around the 15° angle, this trend starts to plateau. Recall Figure 11, for such a highly cambered wing such as this, the direction cosines deviate significantly as much of the wing is functionally operating at a much higher angle of attack. Hence, only a fraction of the local normal force it develops expresses itself as lift.

Similarly, for the first 10°, the increase in drag is not too detrimental. However, above this, it is evident that the drag increase is much more drastic. Once again, recall Figure 11, for such a highly cambered wing such as this, the direction sines deviate significantly as much of the wing is functionally operating at a much higher angle of attack. Hence, a significant fraction of the local normal force expresses itself as drag.

For the test case shown, the 10° results can be found in Figure 20 and Figure 21.

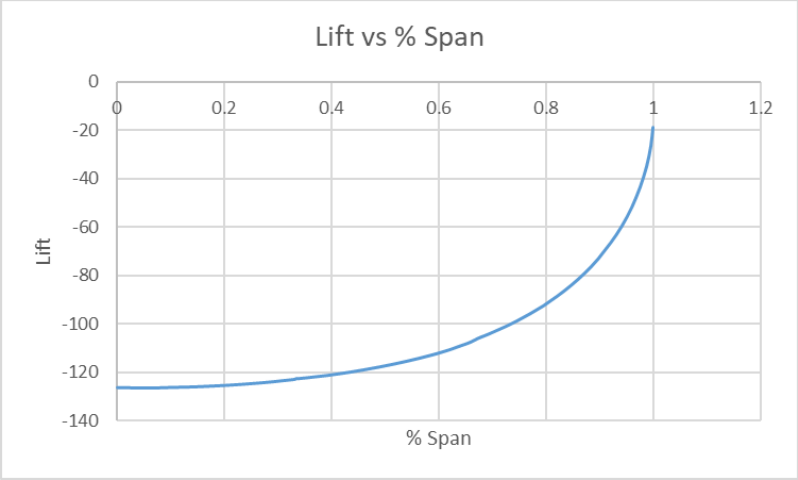

Figure 20: Spanwise Lift Distribution Obtained with a Single Element Front Wing

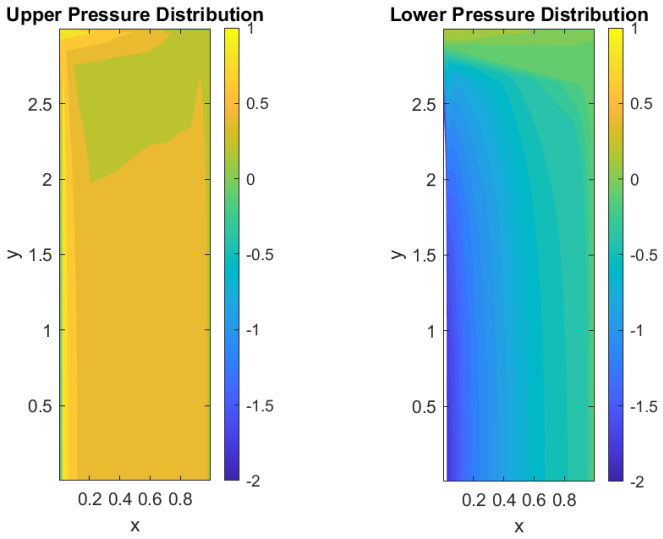

Figure 21: Pressure Contour Obtained with a Single Front Wing

It can be noted in Figure 21 that the flow doesn't generate as much pressure on the upper surface closer to the tip of the wing. So, the next obvious step at this point is to add an endplate at the wingtip to keep the flow attached for longer along the span of the wing as it is clear that pressure is being dumped along the wingtip.

Single Element Wing with Endplates

An endplate was added to the front wing as it was noticed that there were challenges when attempting to hold the pressure generated for longer throughout the span of the wing. This is most likely why cars in the 1980s also added in endplates and cars in 1990s focused some time on improving endplate geometry in order to improve the airflow over the entire wing.

The spanwise lift distribution and pressure distribution obtained for the same wing as earlier (with 10° of incidence) but this time with an endplate added can be seen in Figure 22 and Figure 23.

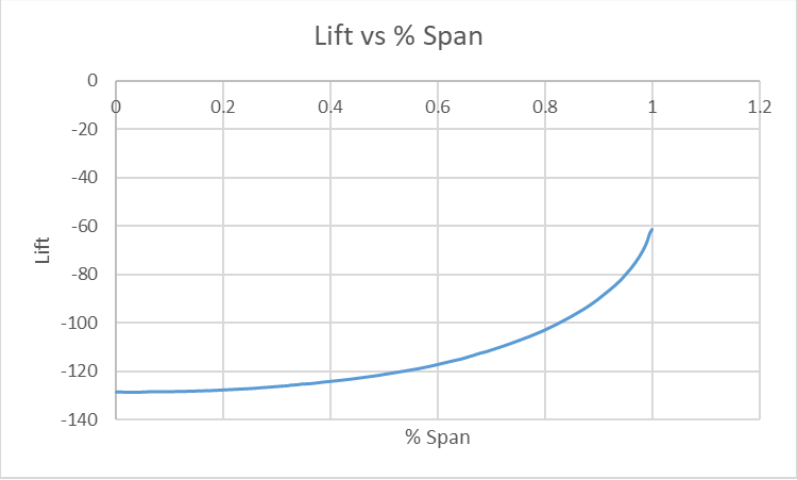

Figure 22: Spanwise Lift Distribution Obtained with Addition of Endplates

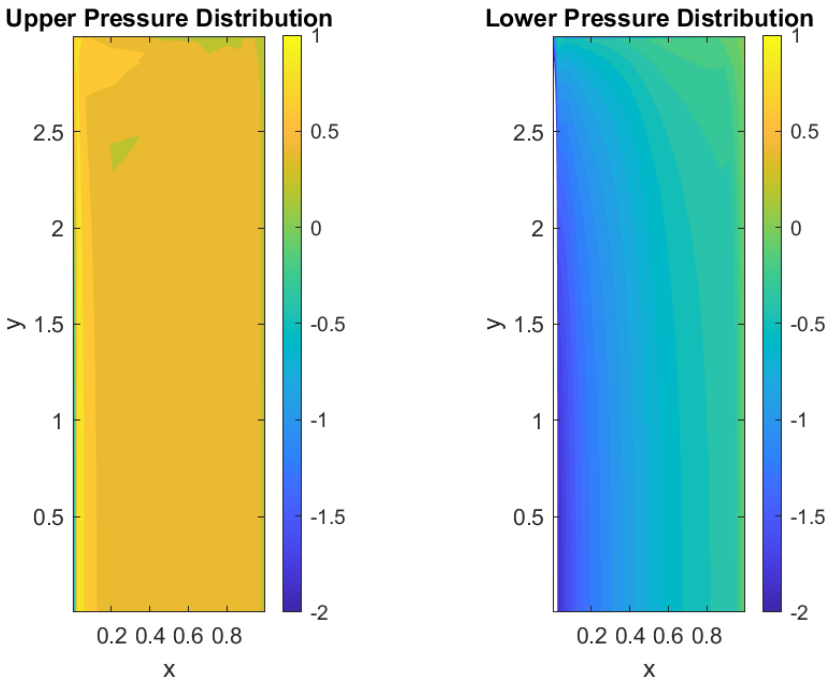

Figure 23: Pressure Contour Obtained with Addition of Endplates

Note in Figure 22, how the spanwise lift distribution does not go down to zero lift at the wingtip anymore. This might not seem like a significant importance, however it is vital that the wingtips generate zero downforce at the wingtips to ensure that sufficient laminar airflow goes to the tires and brakes of the Formula 1 car. So, getting the spanwise lift distribution to an ideal spanwise lift distribution (similar to that of an aircraft ideal spanwise lift distribution but in the downward lift direction) is the challenge that is encountered.

One challenge faced was making sure that the panels did not overlap with one another when developing the panels for the simulation. This resulted in multiple panels used at the endplates to ensure that the lower and upper surfaces of the airfoil. See Figure 24 for a visual representation of this. Note that as the number of wing elements increased,

the number of panels needed for the endplate also increased. For instance, a two-element wing (front and rear elements for one front wing) will require four elements for the endplate (see Figure 33 showing the visualization for a two-element wing).

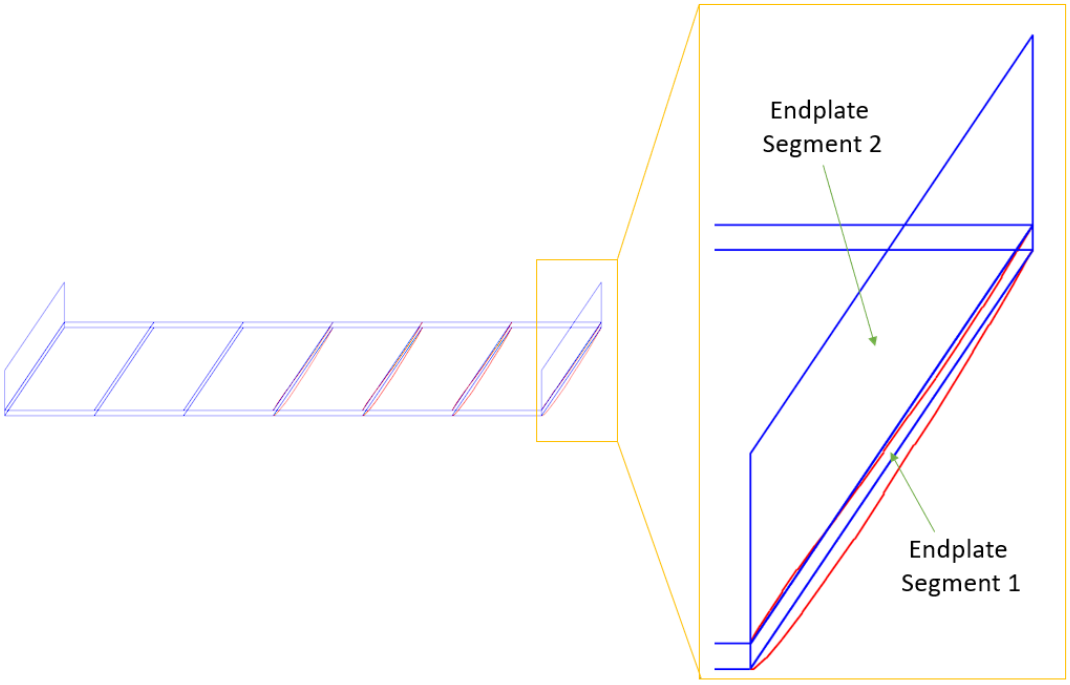

Figure 24: Endplate Visualized for Single-Element Multi-Panel Wing

At this point in the research, it is clear why the next step taken by Formula 1 car manufacturers was to start manipulating the twist in the front wing at various points along the span. By doing so, the spanwise lift distribution can be tweaked to ensure that a spanwise lift distribution similar to that of the ideal spanwise lift distribution can be created. This would significantly improve the grip and braking performance of the Formula 1 car.

An additional note at this point needs to be mentioned to minimize confusion. Note that the area of the wings in all the wings synthesized for this research were held constant to be able to compare with one another in more detail. So, it might seem that Formula 1 cars in the past cars were generating enormous amounts of downforce, but the fact is that the area of front wings in the 70s and 80s were significantly smaller.

EXCEL Solver

For the next stages of the research conducted, multiple EXCEL Worksheets were generated to assist in the solution of the twist and camber parameters. Multiple methods were tested to see which multipliers work best for each of the control points. Of the many tested, the most feasible was the *GRG Nonlinear* solver (Frontline Solvers, 2021) with a penalty function followed by the user tweaking the functions further to obtain the required lift and pressure distributions. The GRG nonlinear solver is a gradient based solver that attempts to minimize a target value (for this research, the error squared value seen in equation 15) by varying specific values on the EXCEL spreadsheet (twist, camber and angle of attack multipliers for this research). It's important to note that the GRG solver has issues with not reaching a satisfying result in some cases which led to tweaking equation 15 to add in constraints and bias factors.

In order to automate the synthesis of the front wing, a penalty function needs to be defined. Equation 15 below shows the equation that was utilized for most cases in the solutions that were run.

$$R^2 = C_1 * \left(\frac{Lift - Ideal\ Lift}{Ideal\ Lift}\right)^2 + C_2 * \left(\frac{(0.8 * Critical\ Pressure) - Pressure}{0.8 * Critical\ Pressure}\right)^2 + C_3 * \left(\frac{Min\ Pressure\ Location - 0.15}{0.15}\right)^2 \quad (15)$$

The first portion of the equation ensures that the spanwise lift distribution is as close as possible to the ideal spanwise lift distribution that was generated. This target spanwise lift distribution can be modified as needed to achieve higher or lower lift in certain portions of the wing.

The second portion of Equation 15 ensures that the critical pressure is not reached by targeting the minimum pressure along each chord section is approximately 80% of that of the critical pressure predicted using Küchemann's critical pressure equation.

The final portion of Equation 15 ensures that the minimum pressure along each chordwise section occurs around the 15% of the chord to attempt to create peaky type conditions for the wing and to generate wing designs with no lumpiness to its pressure distributions.

It can be noted however that there were bias factors applied to each portion of the equation using $C_1, C_2\ and\ C_3$. Generally, there was a higher bias factor applied to the first portion of Equation 15 which focuses on the spanwise lift distribution along the spanwise direction as this is the more vital challenge to the problem a hand.

For a three-panel wing, the linear superposition for twist, camber and incidence can be described as:

$$\frac{L}{q} = k_1 * CNC_{TWIST,CP1} + k_2 * CNC_{TWIST,CP2} + k_3 * CNC_{TWIST,CP3} + k_4 CNC_{TWIST,CP4} + k_5 * CNC_{CAMBER,CP1} + k_6 * CNC_{CAMBER,Cp2} + k_7 * CNC_{CAMBER,CP3} + k_8 * CNC_{CAMBER,CP4} + k_9 * CNC_{INCIDENCE} \quad (14)$$

where $\frac{L}{q}$ *is Lift per Dynamic Pressure, CNC is the spanwise running load, the CP is the control point and the k values are the multipliers for the control point.*

Python for Input File Generation and Running VORLAX

When running the files on VORLAX, there were many errors that had to be understood and rerun multiple times to ensure that the scenarios that were tested were in fact the geometry that were expected to be. Some of these errors made and adaptations are discussed in later sections of the METHOD section.

In order to expedite the batches of files that were created and run the files on VORLAX, a Python script was created. This was not very complicated but involved the parsing of the twist and camber perturbations into each control point and perturbing one control point at a time, one example seen in Figure 28, and each case run on VORLAX individually.

Single Element Wing with Varying Twist

Then, changes in camber and twist were applied by splitting the front wing into three different sections so that more control can be taken in the design of the front wing. This is similar to those representing wings from the 1980s (Figure 3). Four control points were utilized to change the twist of the wing at each control point as seen in Figure 25. Once again, note that control points in the context of this thesis represent the geometry design control point, not grid density control point. Four control points were deemed sufficient as seven were sufficient for the research conducted on airplane wings, but the lack of a Yehudi or significant change in planform, meant that four control points were sufficient to control the spanwise lift distribution of the wing. This essentially gives one control point at the centerline of the wing, one control point at the wing tip and two control points in between the centerline and wingtip allowing for sufficient variation in twist and camber in the wing.

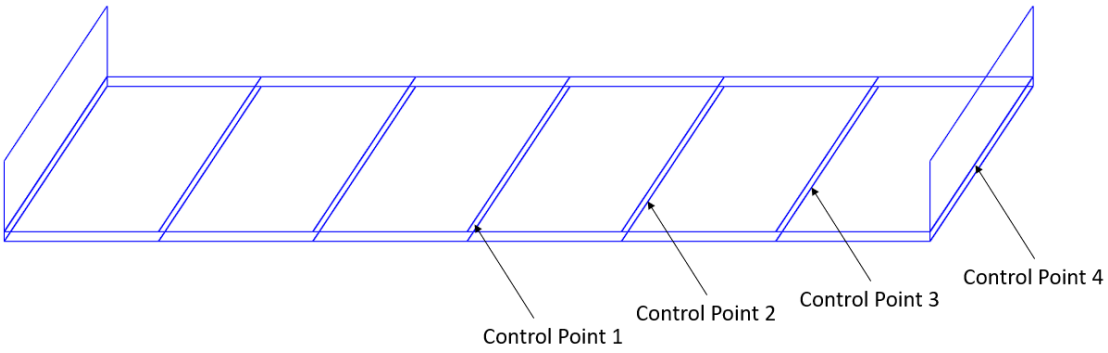

Figure 25: Four Control Points Used to Alter Wing Geometry

This resulted in the spanwise lift distribution seen in Figure 26 where it is visible that the expected spanwise lift distribution and obtained spanwise lift distribution match

very well throughout the span of the wing. More importantly, the lift generated at the wingtip has now been reduced to zero, which can help in the reduction of turbulent air directly in front of the wheels.

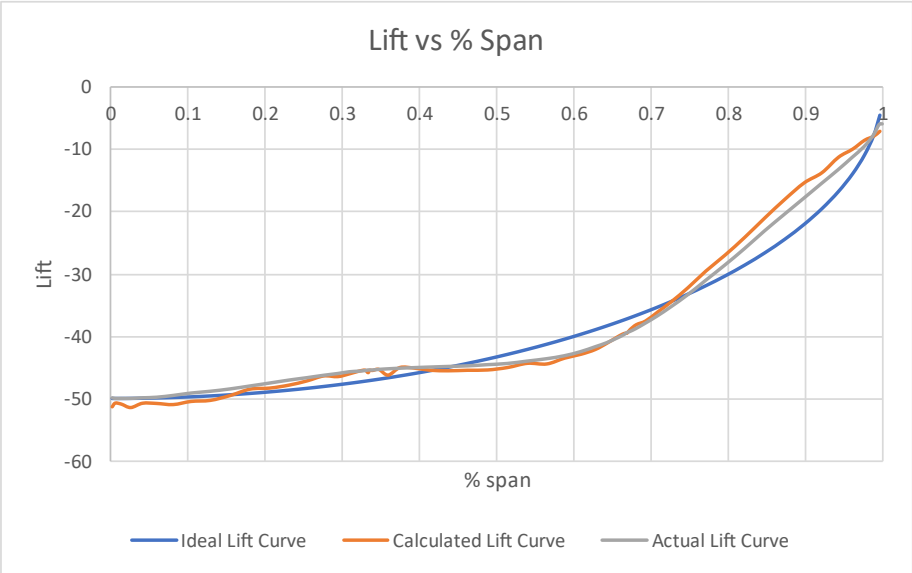

Figure 26: Spanwise Lift Distribution Obtained with Varying Twist Single Element Front Wing

Note that the objective of the solver algorithm was to:

1. Minimize the error between a target spanwise lift distribution (seen in blue in Figure 26) and current spanwise lift distribution,
2. Limit minimum pressure on lower surface to 80% of the critical pressure obtained using Küchemann's critical pressure equation,
3. And locate the minimum pressure to15% of the chord length.

Note that there were bias factors used to favor the first criterion as seen in equation 15.

Single-Element Wings with Multiple Camber and Twist Variations

The next step in this research was to analyze a single element wing with various twist and camber geometries applied. This is somewhat in between the 1990s and 2000s front wings that Formula 1 had.

See Figure 27 for a visualization of the four control points used on the swept single element front wing.

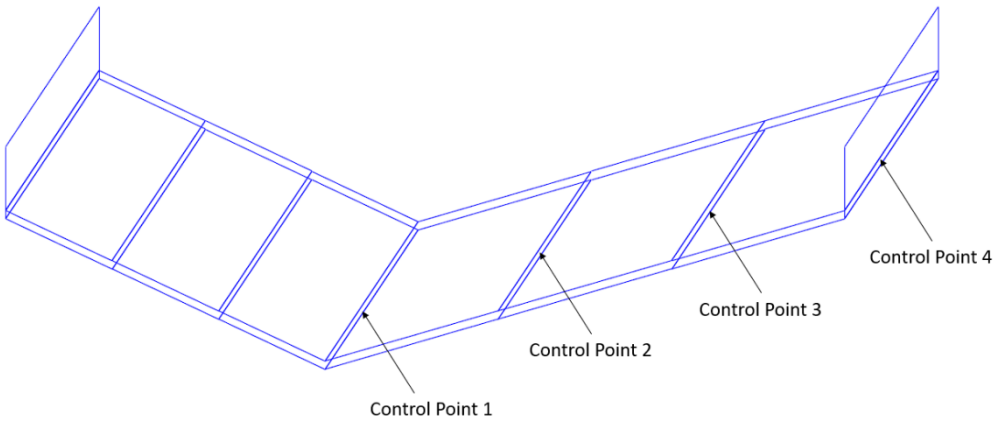

Figure 27: Control Points and Geometry for Twist and Camber Variation on Single Element Front Wing

When attempting to synthesize this wing, the solver kept adding camber towards the ends of the wing resulting in thicker profiles at the tips of the wings. This is not the best scenario in real life as ideally, the center of the wing needs to be thicker and get thinner while going in the spanwise direction to ensure that the support structures on the inside of the wing are strong enough to support the outer structures of the wing. As a result, the cambers at each control point were fixed to ensure a more reasonable camber

distribution and only twist was altered to achieve the required lift and pressure distributions.

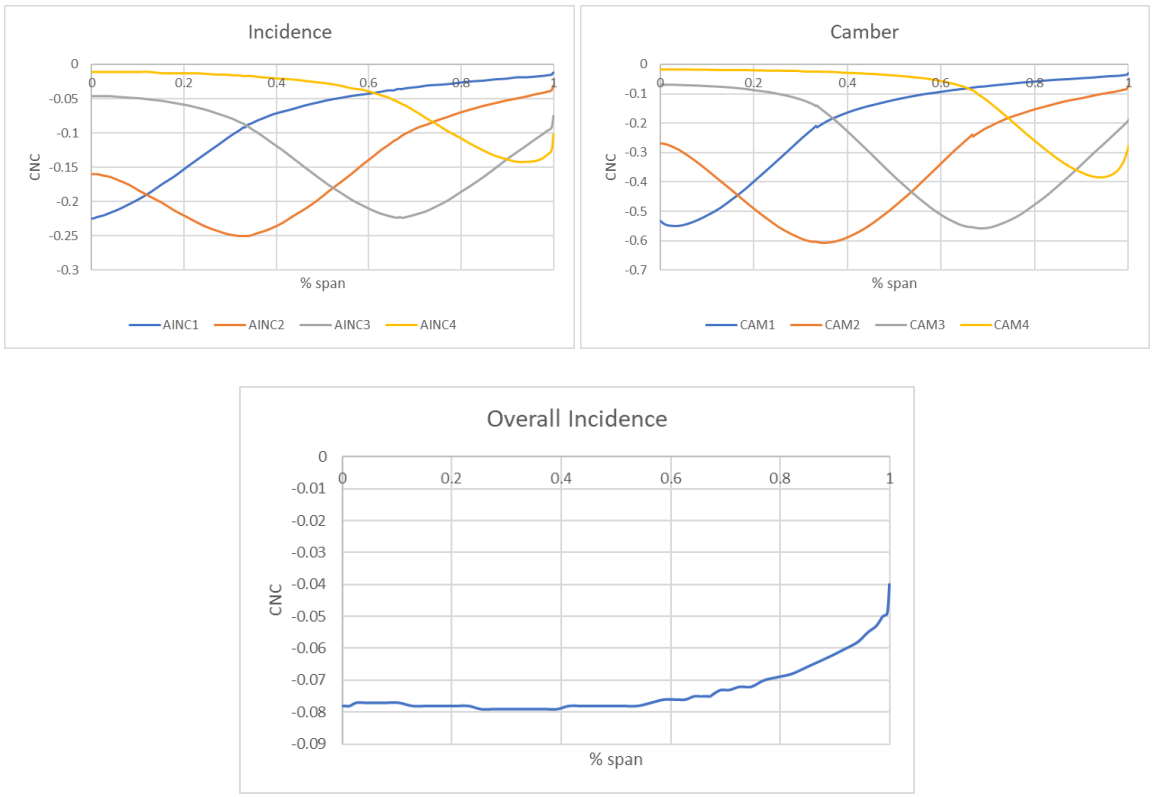

Figure 28: Perturbations of Twist and Camber Visualized

This provided the lift and pressure curves seen in Figure 29 and Figure 30.

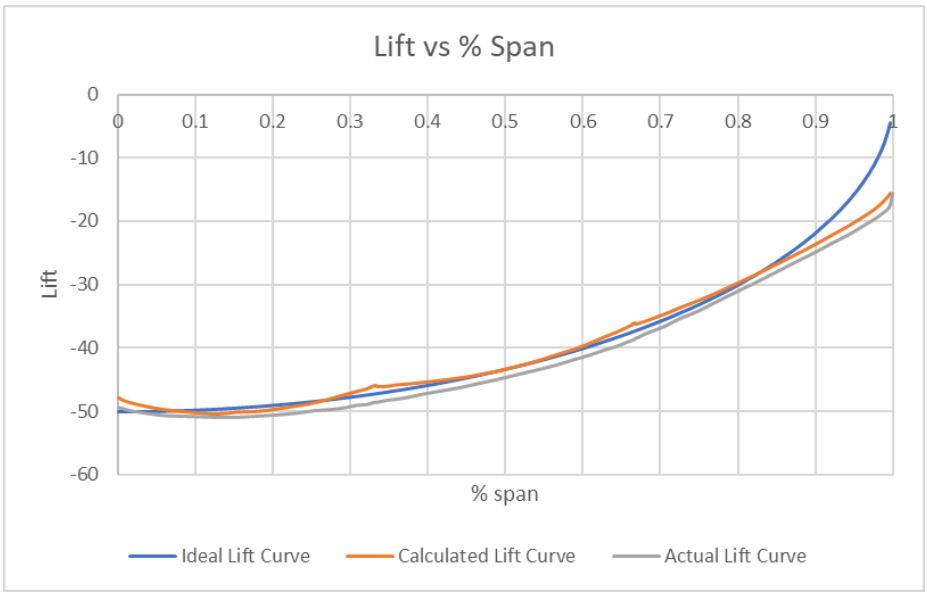

Figure 29: Spanwise Lift Distribution Obtained for Varied and Camber in a Single Element Wing

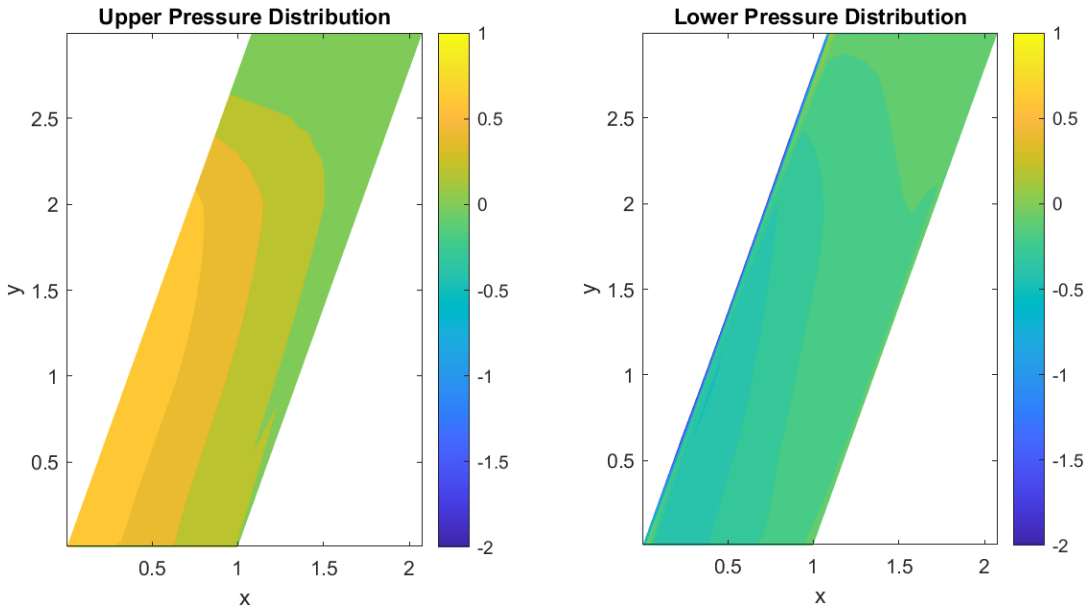

Figure 30: Pressure Contour Obtained for Varied Twist and Camber in a Single Element Wing

It can be seen from Figure 29 and Figure 30 that satisfactory lift and pressure distributions were achieved for the synthesis that was conducted for a three-panel front wing. The spanwise lift distribution is satisfactory in that it follows the ideal spanwise lift distribution for most of the spanwise direction. The only significant deviation that occurs is at the wingtip which is due to the inability to dump all the lift generated (even with some twist applied in the opposing direction as seen in Table 1).

The pressure distribution is satisfactory such that there is no unexpected lumpiness of pressure occurring along the surface of the wing and there is no flow separation occurring based on Küchemann's criteria.

The parameters obtained for this wing can be seen in Table 1.

Table 1: Parameters Obtained for a Single Element Wing

Control Point	Camber	Angle of Incidence in Degrees
1	50%	-1.72
2	40%	-1.15
3	30%	-1.15
4	20%	1.72

Challenges with Varying Twist and Camber

One of the first issues with using panel methods and superposition was seen at this stage. As superpositions principles were used to rapidly synthesize the wing designs, it was observed that camber was not superposing as expected (similar to the case with airplane wings that I observed in work published in 2022. This is because as the camber profile is multiplied by the expected factor to achieve the target spanwise lift distribution

and pressure distribution, the shape of camber changes as a result of direction cosines changing at each control point. See Figure 11 for a visualization of this.

A way to overcome this problem was a two-step synthesis where once the first step was completed to obtain the predicted parameters, the perturbations were simulated again at the expected levels so that the 2nd iteration leads to solutions being closer to the expected lift and pressure contours as a result of the direction cosines not being as different now.

Issues with Multi-Element Wing Synthesis

The next step was to create a two-element wing with varying twist and camber. However, this proved to be somewhat challenging. The first attempt was to synthesize both front and rear elements of the front wing at the same time. However, this proved to be counterintuitive as the solver kept twisting and cambering the front and rear elements in opposite directions to try and achieve the required distributions. This meant another step needed to be taken to obtain the required results.

So, the workaround was to initially synthesize a satisfactory front element of the front wing with parameters set only for the front element. Once this was obtained, the rear wing elements were added and perturbed and a second solver was run to obtain the required pressure and spanwise lift distributions. These steps are explained in more detail in the following sections.

This lines up with what Katz (Katz, Automotive Aerodynamics, 2016) discusses in his textbook as there seems to be very large interactions between the elements that are close to one another leading to a direct synthesis to be unfeasible.

Synthesis of the First Element of a Two-Element Front Wing

As mentioned in the earlier section, the first step required was to synthesize the front-most element of the front wing. This was done the same way as for a single element wing with only the planform of the wing changing now to reflect the change in geometry.

This provided with the following lift and pressure distributions seen in Figure 31 and Figure 32.

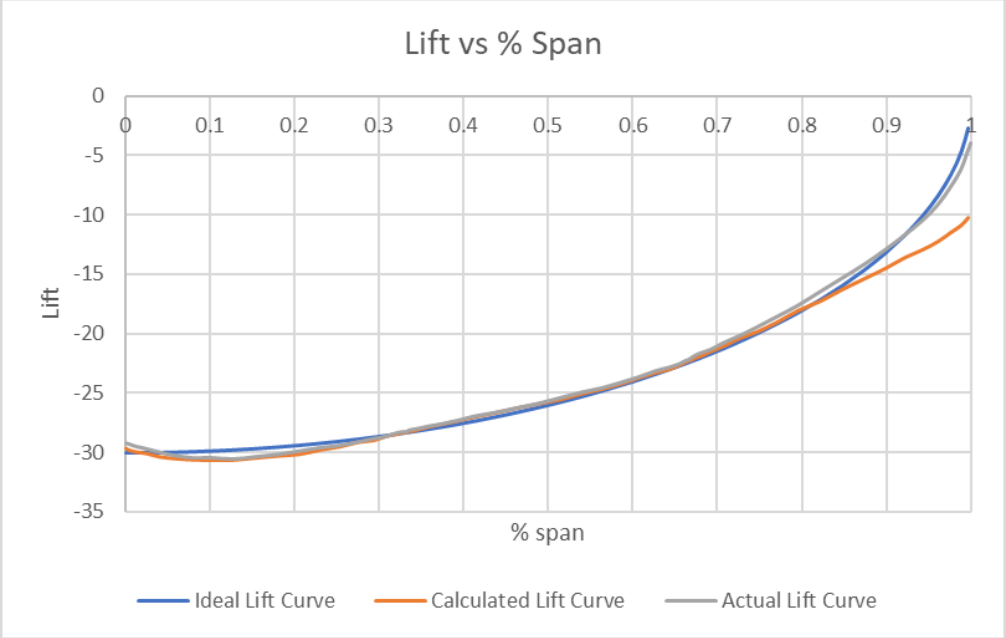

Figure 31: Spanwise Lift Distribution for a Single Element of a Two Element Wing

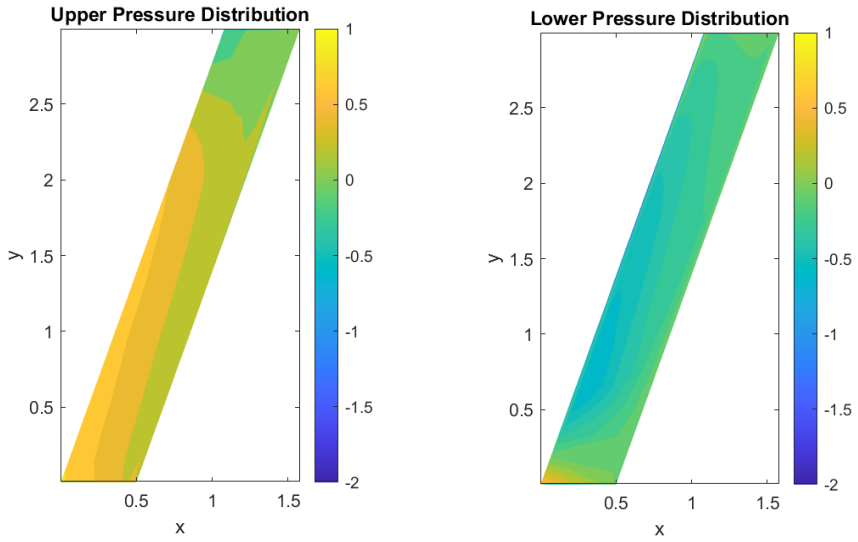

Figure 32: Pressure Distribution for a Single Element of a Two Element Wing

The parameters obtained during this synthesis can be seen in Table 2.

Table 2: Parameters Obtained for a Single Element in a Two Element Wing

Control Point	Camber	Front Angle of Incidence in Degrees
1	50%	-2.29
2	40%	-1.15
3	30%	-1.15
4	20%	1.15

Second Element Synthesis in a Two Element Front Wing

The resulting parameters from the first element synthesis were then fixed and the required control points for the rear element of the front wing were perturbed. The control points for the rear element can be seen in Figure 33.

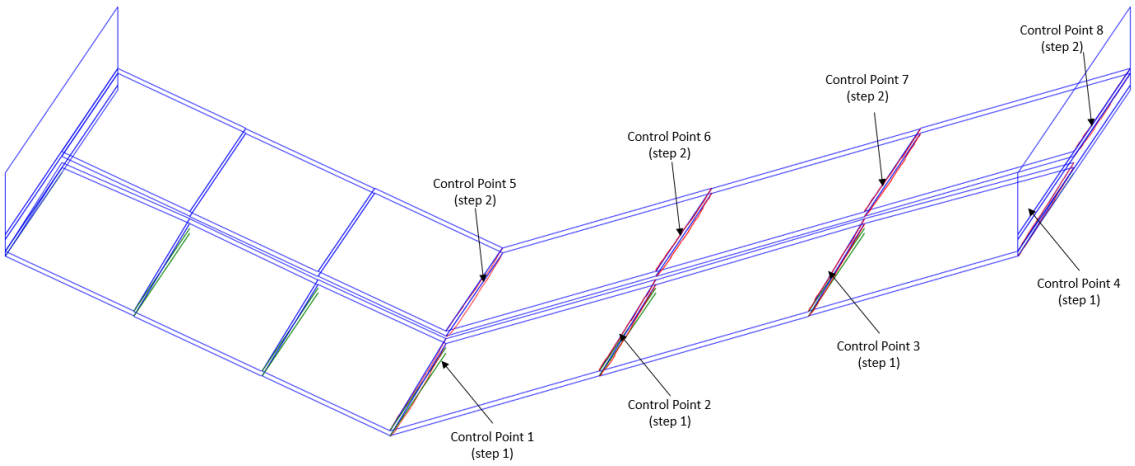

Figure 33: Rear Element Control Points for a Two Element Wing

Using these control points, the following lift and pressure distributions were obtained as seen in Figure 34 and Figure 35.

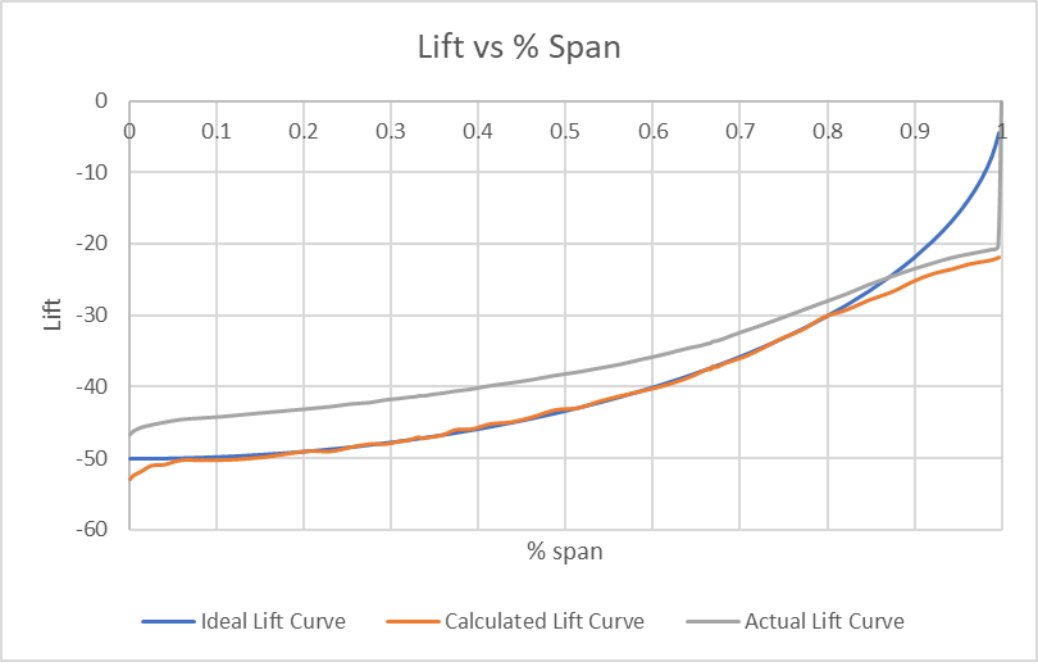

Figure 34: Spanwise Lift Distribution for a Two Element Wing

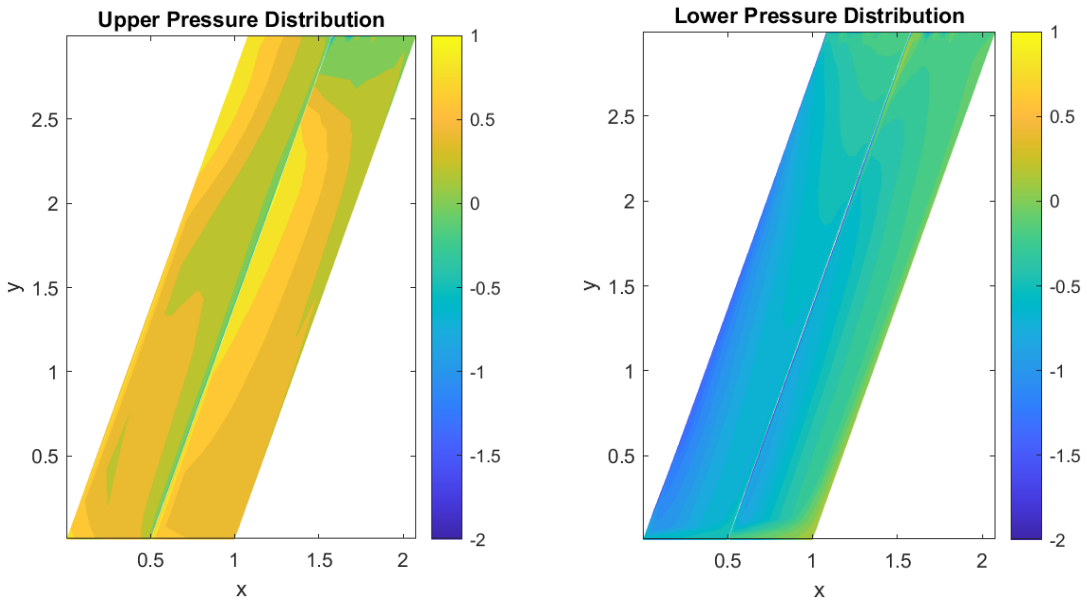

Figure 35: Pressure Distribution for a Two Element Wing

Table 3: Parameters Obtained for a two-element Wing

Control Point	Camber	Front Angle of Incidence in Degrees	Rear Angle of Incidence in Degrees
1	50%	-2.29	-16.70
2	40%	-1.15	-12.95
3	30%	-1.15	-10.20
4	20%	1.15	0.00

Unfortunately, when it came to perfecting the spanwise lift distribution for the final steps, this needed to be done by intuition and trial and error. I guess AI cannot take over all our jobs just yet! But in all seriousness, this was an interesting find for me. When working on airplane wings that only had variation across the spanwise length (and in the case where only a single element was synthesized as shown in this thesis), the algorithm on EXCEL which is based on superposition was able to be run twice to achieve the required spanwise lift distribution and pressure distribution, accurately. However, when

utilizing multiple elements (as in two-elements in a wing, even when only varying one element parameters), the algorithm had trouble finding a satisfactory solution.

There were various parameters tested with the penalty function to attempt to find a satisfactory workaround for this, however, there was no feasible penalty function observed that corrected for this error.

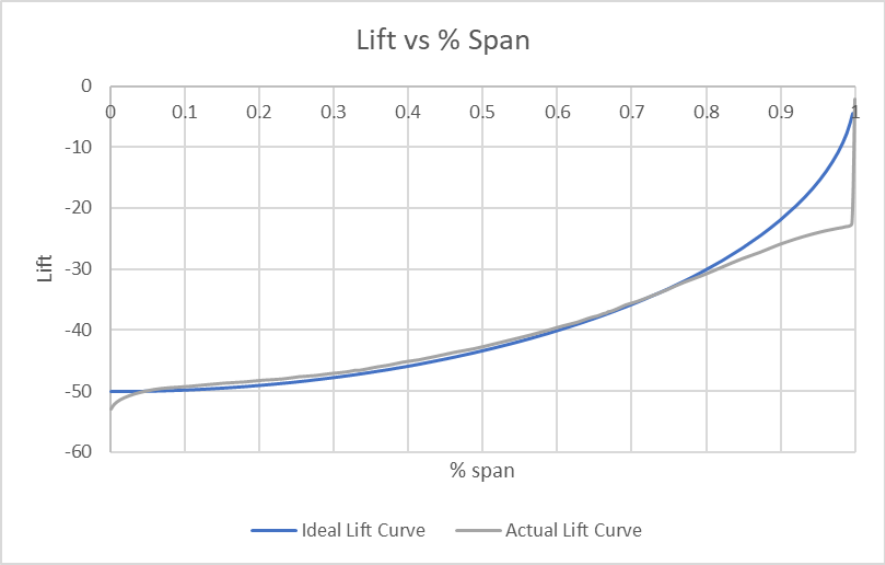

Figure 36: Corrected Spanwise Lift Distribution for two-element Wing

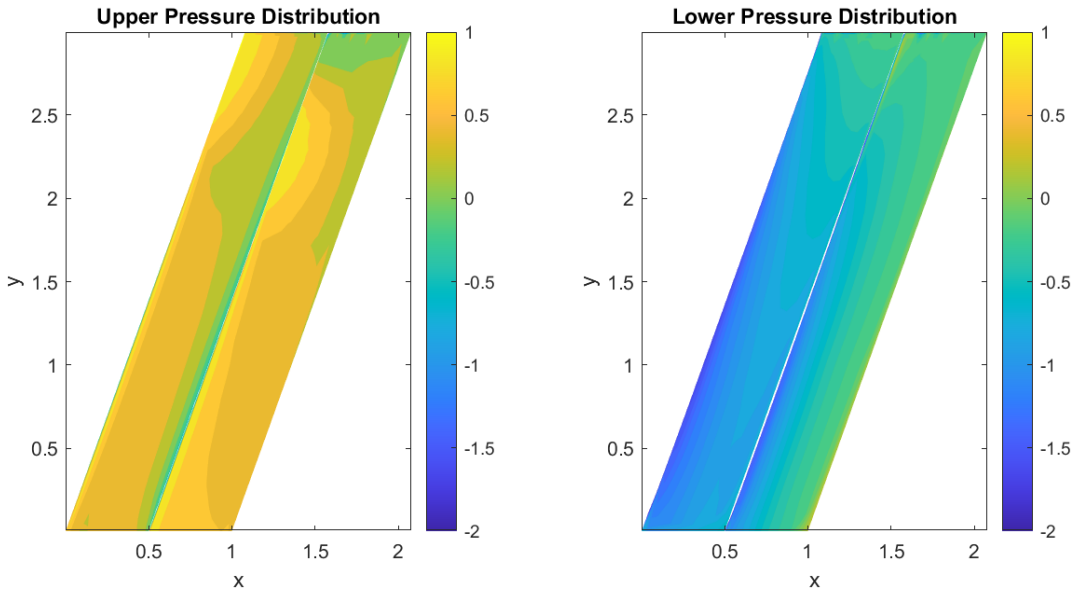

Figure 37: Pressure Distribution for a Corrected two-element Wing

Table 4: Parameters Obtained for a Corrected two-element Wing

Control Point	Camber	Front Angle of Incidence in Degrees	Rear Angle of Incidence in Degrees
1	50%	-2.29	-21.31
2	40%	-1.15	-16.70
3	30%	-1.15	-13.50
4	20%	1.15	0.00

Limitation of VORLAX and Panel Methods

At this stage, a limitation of panel methods was realized as it was not feasible to create wing designs with smooth flowing structures such as the front wings seen in the 2022 Formula 1 car (Figure 7). This is because VORLAX is only capable of having geometries that are straight edged in terms of planform.

Alternate Shapes

However, there was still a lot to learn from the geometry of the planform. So, there were three additional cases run with the same parameters to see how the shape of the wing comes into play. The three cases were:

1. Having a straight leading edge – no sweep on the wing,
2. Overlaying wings – a portion of the rear element is over the front element of the wing, and
3. Increased gap wings – the gap between the first and second elements was increased.

The following sections discuss this in more detail.

Straight Leading-Edge

Figure 38 shows the geometry of the straight leading-edge (or upswept) wing tested.

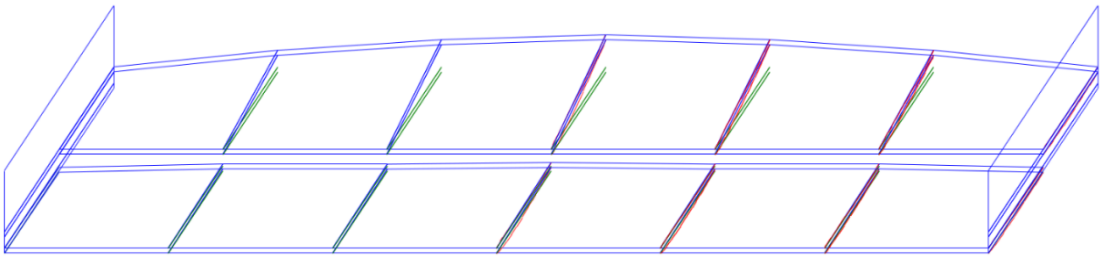

Figure 38: Straight Leading-Edge Geometry

This case gave the spanwise lift distribution and pressure distributions seen in Figure 39 and Figure 40.

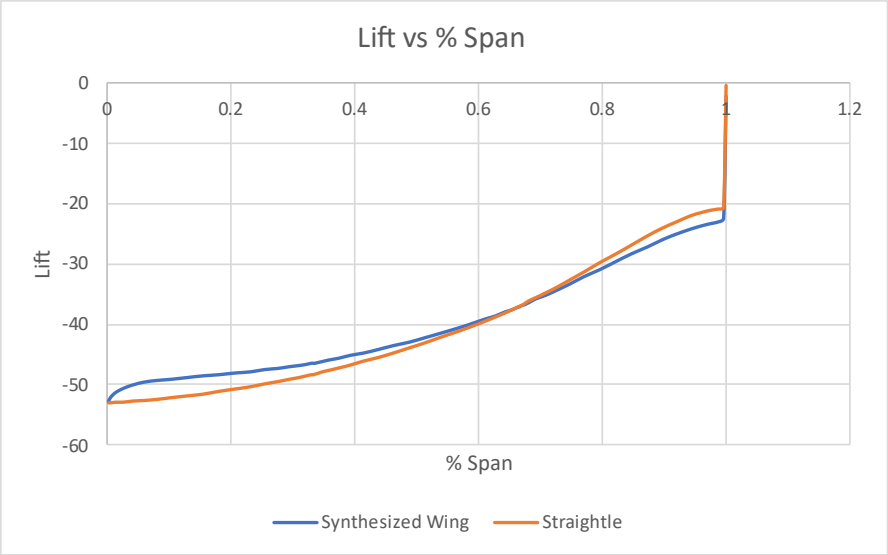

Figure 39: Spanwise Lift Distribution Obtained for a Straight Leading-Edge Wing

It can be noticed that the lift generated in the case of the synthesized wing (with sweep) and straight leading-edge were comparable.

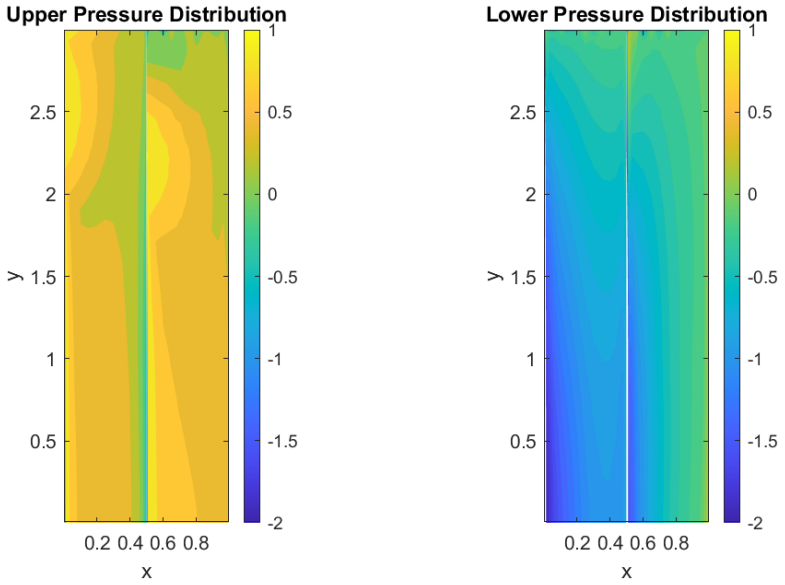

Figure 40: Pressure Contour Obtained for a Straight Leading-Edge Wing

However, the pressure distributions tell another story. It is clearly noticeable that the wings with no sweep have a higher pressure seen at the front edges of the wing with a straight leading edge are higher than that seen in the swept synthesized wing. This is consistent with that discussed by Ackeret, Degen and Rott (Ackeret, Degen, & Rott, 1951), where they observe similar phenomenon. This is also consistent with the evolution of Formula 1 front wings where up until 2016, the Formula 1 wings all had straight leading edges. But in 2017, the designs started to sweep and in 2022, the sweep was drastically increased. The swept wing helps to minimize the leading-edge pressure which results in a reduction of flow separation at the leading edge of the wing.

This is of course standard knowledge in aircraft design and was discussed in work published in the early 1950s (Ackeret, Degen, & Rott, 1951). But it took till 2017 for these ideas to enter the Formula 1 aerodynamics, although some of the reasoning could be due to the heavily regulated designs by the FIA on what the Formula 1 car can look like.

Overlaying Wings

One more case that was tested was the overlaying wings, where the rear element started above the front element before the front element chord length was finished. What this led to is the front element not being completely exposed to open air in the trailing edge.

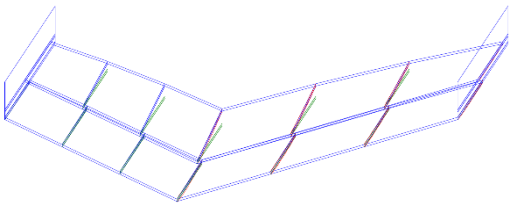

Figure 41: Geometry for Overlaying Wings

This gave the spanwise lift distribution seen in Figure 42. As observed below, the lift obtained was reduced due to less overall surface area being exposed to the open air. Once again, this is consistent with what is observed in current generation Formula 1 wings where the different elements of the front wing start just above the previous element in front. While it may look like there is some overlap, the elements are actually in such a way that there is minimal overlap, and the outer ribs are connected the trailing edge of the front element to the leading edge of the rear element.

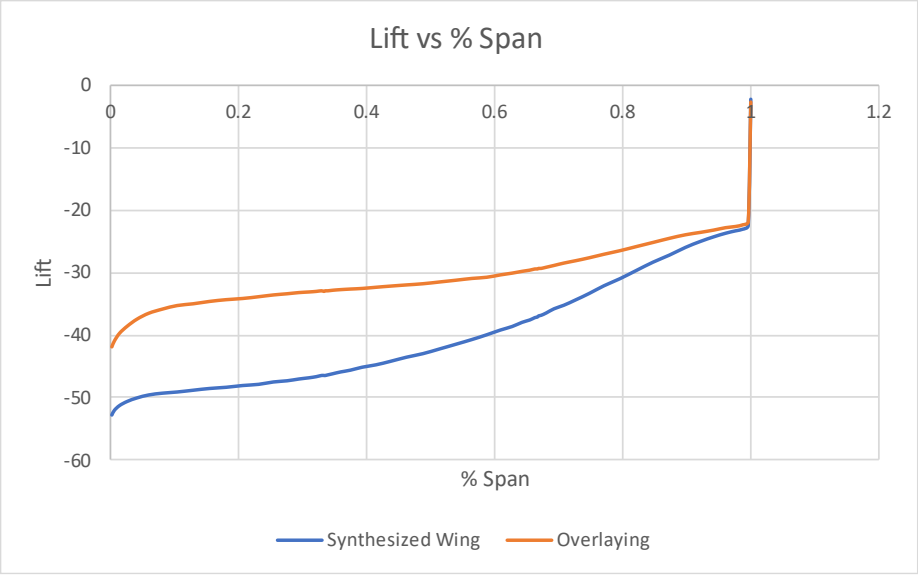

Figure 42: Spanwise Lift Distribution Obtained for Overlaying Wing

The pressure distribution for the overlaying wings can be seen below in Figure 43.

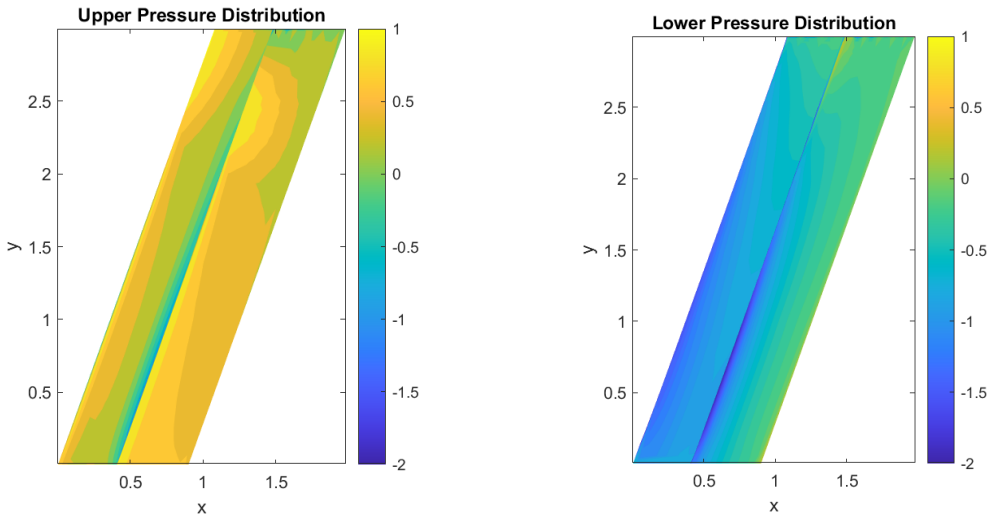

Figure 43: Pressure Contour Obtained for Overlaying Wings

Increased Gap Wings

To see if there was an effect by increasing the gap between elements, the increased gap wing case was tested. See Figure 44 below for the geometry.

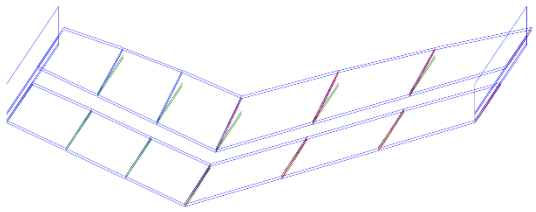

Figure 44: Geometry for Increased Gap Wings

This gave the spanwise lift distribution seen in Figure 45. It can be noticed that in this case, the case between the synthesized wing and increased gap wing was minimal.

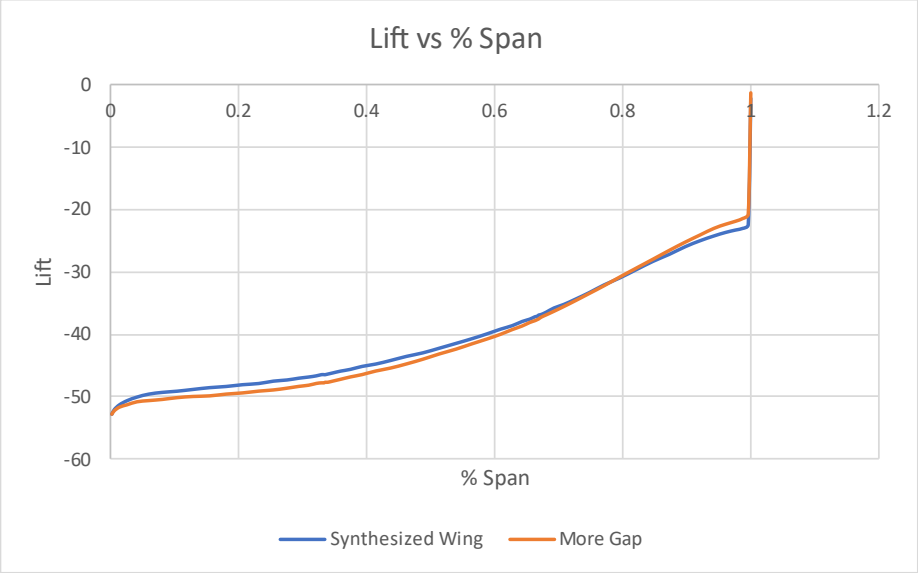

Figure 45: Spanwise Lift Distribution Obtained for Increased Gap Wings

The pressure distributions for this case can be seen below in Figure 46.

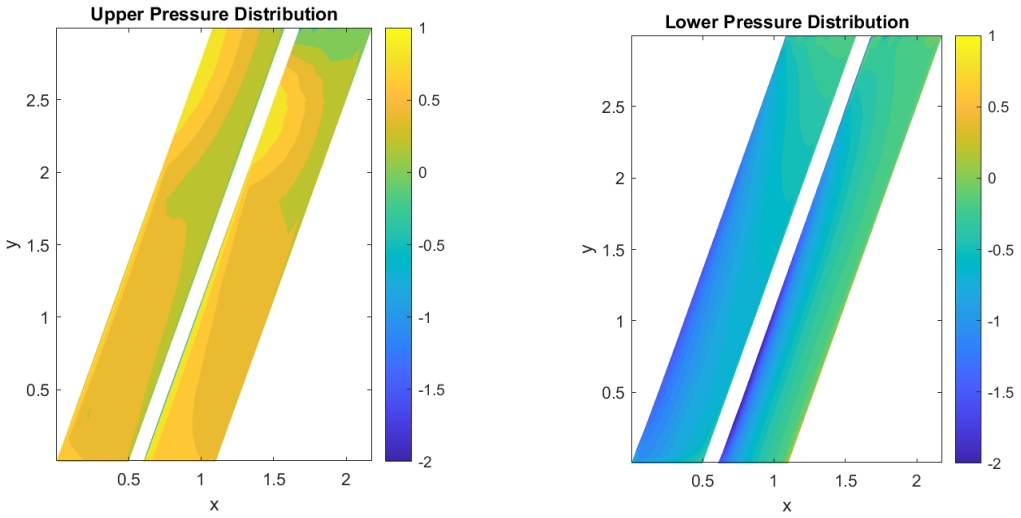

Figure 46: Pressure Contour Obtained for Increased Gap Wings

Notice that the pressures seen at the leading edge of the rear element is higher in this case because the highly twisted rear element is now exposed to open air as opposed

to the synthesized wing having more airflow coming to it after being redirected by the front element.

CHAPTER 4

RESULTS

To better understand the lift and drag characteristics of the wings mentioned in the earlier section, a table was created to observe the various coefficients of lift and inviscid pressure drag for each case.

Table 5: Comparing Coefficients of Lift and Drag

	Synthesized Wing	Straight LE	Overlaying	More Gap	Single Element
Coefficient of Lift	-0.96355	-0.99447	-0.88508	-0.98047	-0.40691
Coefficient of Drag	0.09888	0.10134	0.09956	0.10459	0.00909

It can be seen in Table 5 that each wing that was compared has its own benefits. Comparing the straight leading edge with the synthesized wing shows that the coefficient lifts in both are comparable. However, it is important to note that the pressure distributions of the two wings are different. Figure 37 and Figure 40 show these differences clearly on the contour plots. So, even though it might seem that the straight leading-edge wing has an advantage when looking at Table 5: Comparing Coefficients of Lift and Drag, other factors from previous discussions need to be considered as well.

The overlaying wing can be seen to be less beneficial as it is clear that the coefficient of lift is less, and coefficient of drag is more for the overlaying wing when compared to the synthesized wing.

The wing with more gap in between the front and rear elements seems to be superior to the synthesized wing when looking at Table 5, however recall that the increased gap wing has higher leading-edge pressure which could lead to quicker flow separation, especially under heavy loading scenarios such as turning.

The single element wing generates lesser coefficient of lift and lesser coefficient of inviscid drag, but it is important to recall that this is only using the same parameters as the two-element wing. This wing can be optimized to be comparable to the synthesized wing performance, however, the inviscid drag experienced will be significantly more at these conditions for the single element wing.

Runtime Discussion

The runtimes for VORLAX and the EXCEL solver are as follows:

- VORLAX panels for the two-element wing with camber, incidence and angle of attack took approximately 4.75 seconds,
- VORLAX panels for a single-angle-of-attack / single-Mach-number solution for a simple perturbation of camber or twist took approximately 0.50 seconds,
- EXCEL GRG Nonlinear Solver for twist only took approximately 4.50 seconds,
- EXCEL GRG Nonlinear Solver for twist, camber and angle of attack took approximately 19.50 seconds.

As it can be seen from the times above, the runtimes for the algorithm developed in this research is very small especially when compared to running simulations using finite volume methods. This gives the method discussed in this thesis a significant advantage when it comes to scenarios where rapid synthesis is required or in cases where computing power might be limited. This is especially useful in scenarios such as rapid testing for race weekends, especially in free practice where multiple panels can be tested to predict what setup to run on the race car prior to sending the car onto the track. This

method could also be beneficial for student teams in Formula SAE so that an initial design can be synthesized without using finite volume methods which take significantly longer to run and require high system specifications to run the simulations.

CHAPTER 5

VERIFICATION

The goal of this section was originally to simulate a select number of wings synthesized on ANSYS Fluent so that a direct comparison could be made. However, there were multiple issues that were faced for this process. In order to obtain results that are reliable and accurate, the grid elements need to be sufficiently small so that the physics can be modelled accurately. However, with the student license available to ASU students, there is a limitation on the number of nodes that can be allocated for each simulation (512, 000 nodes maximum). Even with the ANSYS version available on Apporto, while this may look like the full version of ANSYS at first, when fully loaded, it is clear that the node limit still applies as the loading screen shows the limitations of the student version.

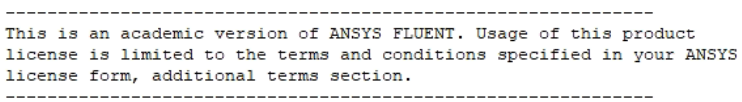

Figure 47: ANSYS Student Version on Apporto

As a result, the simulations run did not converge as much as I preferred due to the limitation on the number of nodes. The settings used for ANSYS can be seen in Table 6.

Table 6: Settings for ANSYS Fluent Simulations

Method	SIMPLE
Viscous Model	k - ω SST
Fluid	Air
Inlet Velocity	85 m/s
Airfoil	Stationary wall
Floor Velocity	85 m/s
Symmetry	Through center of the wing

Figure 48 shows the SolidWorks model designed of the six-element front wing that was synthesized to run simulations on ANSYS.

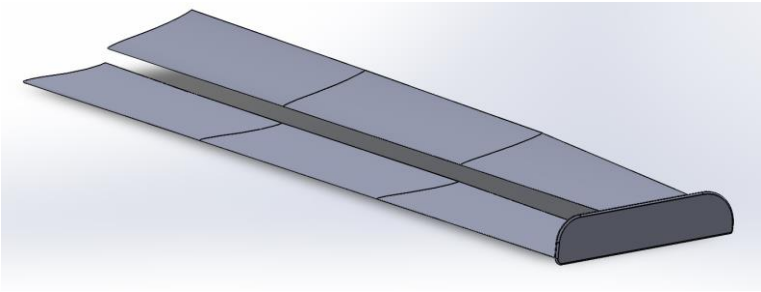

Figure 48: SolidWorks Model of Six-Element Wing for ANSYS Simulations

Unfortunately, due to restrictions of the student license, I was unable to obtain satisfactory results to compare with the results obtained from panel methods as significantly more nodes are required to model the interaction between wing elements that are very close to one another and to model the ground effect which is not taken into account in panel methods.

Recommendations and Observations

This portion is mostly for my future self so that I won't make the same mistakes in the future. ANSYS is a great tool but requires a lot of patience and computing power. For students like me who don't have access to high performance computing, ASU offers cloud computing on Apporto with some impressive specifications for no extra charge. However, getting Apporto to work smoothly was challenging. Apporto requires a very stable internet connection and is very dependent on continuous connectivity. It was impossible to run over WiFi and required a plugged in ethernet connection in my experience and even then, the lag when controlling the machine was very visible.

The workaround for this was creating the SolidWorks model on my desktop and then exporting an Initial Graphics Exchange Specification (.iges) file to ANSYS on Apporto. This file can then be imported on ANSYS and an enclosure can be added for modelling (my preference was Design Modeler for the sole reason that it was the modeling software that I learned during my undergraduate program at Arizona State University). Afterwards, the model has to be meshed very carefully to ensure that there is sufficient resolution to model the interactions between wing elements. Unfortunately, this easily went into the 700, 000 nodes region for a sufficient model for the synthesized wing design, which was above the 512, 000 nodes maximum available on the student license. The designs with lesser resolution meshes tend to give unexpected artefacts such as unexpected regions of high pressure on the lower surface of the wing.

My recommendation for myself in the future and any students working on the student license of ANSYS is to understand the limits early on, rather than trying to keep

getting it to work. Software such as OpenFOAM can be very frustrating to set up but has no limitations as it is open source. So, for students with budget restrictions, this might be a great alternative.

CHAPTER 6

CONCLUSION

It can be noticed that the research that was conducted was consistent with what was seen over the past 50 years for Formula 1 front wings where the flow over the wings were understood over time and different concepts were adapted to improve flow conditions. The evolution starts with attaching endplates to front wings which holds the flow attached for longer along the spanwise direction.

This is followed by using twist to created improved spanwise lift distribution, specifically to load the wing at certain points and to attempt and generate zero lift at the wingtips for better tire and brake performance due to less turbulent flow in those regions.

This brought about the change in camber as well which assisted in weight reduction purposes as well as loading the wing to achieve improved airflow by making the airflow over the wing more laminar.

And more recently, the multi-element wings show that higher lift can be generated with less drag being generated when compared to single-element wings. This allows the current larger Formula 1 cars to generate the downforce required to keep them on track when cornering at high speeds. This is especially important when ensuring that the aerodynamic center of the car falls at a satisfactory location along the car to prevent the car from spinning out especially when cornering or large gusts of wing occur, either due to natural reasons or from the turbulence generated when following cars in the front when overtaking.

REFERENCES

Abbott, I. H., Doenhoff, A. E., & Stivers, Jr., L. S. (1945). *Summary of Airfoil Data, Report No 824.* Langley: NATIONAL ADVISORY COMMITTEE FOR AERONAUTICS.

Ackeret, J., Degen, M., & Rott, N. (1951). *Investigations on Wings With and Without Sweepback at High Subsonic Speeds.* Washington: NACA.

Armenta, F. X., Plaban, P., & Takahashi, T. T. (2022). Revisiting Neumark's Critical Pressure Coefficient Rule for Aircraft with Finite Wings. *AIAA SciTech 2022.* San Diego: AIAA.

Bersy, T. (2012, May 2). *De Tomaso 505*. Retrieved from Flickr: https://www.flickr.com/photos/tautaudu02/7137059557

Bertin, J. J., & Cummings, R. M. (2014). *Aerodynamics for Engineers.* Pearson.

Castro, X., & Rana, Z. A. (2020). Aerodynamic and Structural Design of a 2022 Formula One Front Wing Assembly. *Fluids 2020*.

Cebeci, T., Mosinskis, G. J., & Smith, A. (1970). *CALCULATION OF VISCOUS DRAG AND TURBULENT BOUNDARY-LAYER SEPARATION ON TWO-DIMENSIONAL AND AXISYMMETRIC BODIES IN INCOMPRESSIBLE FLOWS.* McDonnell Douglas Corporation.

Cebeci, T., Mosinskis, G. J., & Smith, A. (1972). *Calculation of Separation Points in Incompressible Turbulent Flows.* AIAA.

Donovan, S., & Takahashi, T. (2010). A Rapid Synthesis Method to Develop Conceptual Design Transonic Wing Lofts. *Multidisciplinary Analysis Optimization Conference.* Fort Worth: AIAA.

emkanicepic. (2019, November 1). *ford-formula-1-race-car-motorsport*. Retrieved from Pixabay: https://pixabay.com/photos/ford-formula-1-race-car-motorsport-4594412/

Frontline Solvers. (2021, September 28). *Excel Solver Online Help*. Retrieved from Frontline Solvers: https://www.solver.com/excel-solver-online-help

Jensen, J., & Takahashi, T. (2016). Wing Design Challenges Explained: A study of Finite Wing Effects of Camber, Thickness and Twist. *AIAA SciTech Forum.* San Diego: AIAA.

Kai, T. (1989). A Survey of Separation Prediction Methods Applied to Potential Flow Simulations for an Airfoil. *Oklahoma State University M. S. Thesis*.

Katz, J. (1996). *Race Car Aerodynamics: Designing for Speed (Engineering and Performance).* Bentley Publishers.

Katz, J. (2006). Aerodynamics of race cars. *Annual Review of Fluid Mechanics*.

Katz, J. (2016). *Automotive Aerodynamics.* John Wiley & Sons.

Küchemann, D. (2012). *The Aerodynamic Design of Aircraft.* AIAA.

Mayer, J. P. (1948). *A Limit Pressure Coefficient and an Estimation of Limit Forces on Airfoils at Supersonic Speeds.* Washington: NACA.

Miranda, L. R., Elliott, R. D., & Baker, W. M. (1977). *A Generalized Vortex Lattice Method for Subsonic and Supersonic Flow Applications.* Langley: National Aeronautics and Space Administration.

motorsport.com. (2017, December 22). *Braking power: What's the biggest stop of the Formula 1 season?* Retrieved from motorsport.com: https://www.motorsport.com/f1/news/braking-power-whats-the-biggest-stop-of-the-formula-1-season/3221934/

Netsyscom. (2016, December 14). *f1-formula-one-ayrton-senna*. Retrieved from Pixabay: https://pixabay.com/photos/f1-formula-one-ayrton-senna-1906649/

Pexels. (2016, March 25). *fast-speed-racing-speedway*. Retrieved from Pixabay: https://pixabay.com/photos/fast-speed-racing-speedway-1281628/

Prandtl, L. (1936). *General Considerations on the Flow of Compressible Fluids.*

randomwinner. (2019, July 16). *charles-leclerc-scuderia-ferrari*. Retrieved from Pixabay: https://pixabay.com/photos/charles-leclerc-scuderia-ferrari-4341624/

Ratnayake, S., & Takahashi, T. (2021). Improved Synthesis Method to Develop Conceptual Design Wing Lofts. *AIAA SciTech Forum.* San Diego: AIAA.

Ratnayake, S., & Takahashi, T. (2023). Low Aspect Ratio High-Lift Wing Design for Automotive Racing Applications. *AIAA Aviation Forum.* San Diego: AIAA.

Selig, M. S., Donovan, J. F., & Fraser, D. B. (1989). *Airfoils at Low Speed.* Virginia Beach: H. A. Stokely.

Smith, A. M. (1975). High-Lift Aerodynamics. *37th Wright Brothers Lecture, VOL. 12, NO. 6*.

Souders, T., & Takahashi, T. (2021). VORLAX 2020: Benchmarking Examples of a Modernized Potential Flow Solver. *Aviation* . AIAA.

Takada, H. (1975). *An Extension to the Critical Flow of Stratford's Theory for Predicting the Turbulent Separation Position.* Nagano: Journal of the Physical Society of Japan.

Toby_Parsons. (2018, February 25). *f1-formula-1-car-f1-car-mercedes*. Retrieved from Pixabay: https://pixabay.com/photos/f1-formula-1-car-f1-car-mercedes-3169297/

Ulv, L. (2019, December 18). *Arrows Supertec A21, 2000 - Barry Walker*. Retrieved from Flickr: https://www.flickr.com/photos/lavulv/49238201023/in/photostream/

White, F., & Xue, H. (2021). *Fluid Mechanics.* McGraw Hill.

Wilson, J. (2017, June 20). *Benetton B190*. Retrieved from Flickr: https://www.flickr.com/photos/47676646@N08/35044428330

APPENDIX A

INPUT FILE FOR FINAL SYNTHESIZED WING

```
VORLAX - TEST TOTAL
*
*ISOLV    LAX      LAY      REXPAR    HAG      FLOATX    FLOATY    ITRMAX
0         0        0        0.2       0        0         0         399
*
*NMACH    MACH
1         0.25
*NALPHA   ALPHA
1         0.0
*
*LATRL    PSI      PITCHQ    ROLLQ     YAWQ      VINF
0         0        0         0         0         1
*
*NPAN     SREF     CBAR      XBAR      ZBAR      WSPAN
16        6.38     0.94      0         0         6
*
*X1       Y1       Z1        CORD1   PANEL 1 UPPER FRONT
0         0        0.015     0.5
0.36      1.00     0.015     0.5
*NVOR     RNCV     SPC       PDL
20        15       0         0
*AINC1    ANINC2   ITS       NAP       IQUANT    ISYNT     NPP
0.040     0.020    1         18        2         0         0
*
* X/C
0
0.337
1.034
3.417
6.959
11.512
16.911
23.157
30.427
38.575
47.37
56.515
65.666
74.446
82.465
89.349
94.754
100
* XLE1
```

1.1
* CAMBER ROOT
0.1725
0.3865
0.535
0.7645
0.893
0.905
0.762
0.3485
-0.252
-0.907
-1.516
-1.993
-2.2715
-2.3125
-2.107
-1.682
-1.096
0
* XLE2
1.1
* CAMBER TIP
0.138
0.3092
0.428
0.6116
0.7144
0.724
0.6096
0.2788
-0.2016
-0.7256
-1.2128
-1.5944
-1.8172
-1.85
-1.6856
-1.3456
-0.8768
0
*
*X1 Y1 Z1 CORD1 PANEL 2 UPPER FRONT
0.36 1.00 0.015 0.5

0.72 2.00 0.015 0.5
*NVOR RNCV SPC PDL
20 15 0 0
*AINC1 ANINC2 ITS NAP IQUANT ISYNT NPP
0.020 0.020 1 18 2 0 0
*
* X/C
0
0.337
1.034
3.417
6.959
11.512
16.911
23.157
30.427
38.575
47.37
56.515
65.666
74.446
82.465
89.349
94.754
100
* XLE1
1.1
* CAMBER ROOT
0.138
0.3092
0.428
0.6116
0.7144
0.724
0.6096
0.2788
-0.2016
-0.7256
-1.2128
-1.5944
-1.8172
-1.85
-1.6856
-1.3456

-0.8768
0
* XLE2
1.1
* CAMBER TIP
0.1035
0.2319
0.321
0.4587
0.5358
0.543
0.4572
0.2091
-0.1512
-0.5442
-0.9096
-1.1958
-1.3629
-1.3875
-1.2642
-1.0092
-0.6576
0
*
*X1 Y1 Z1 CORD1 PANEL 3 UPPER FRONT
0.72 2.00 0.015 0.5
1.08 3.00 0.015 0.5
*NVOR RNCV SPC PDL
20 15 0 0
*AINC1 ANINC2 ITS NAP IQUANT ISYNT NPP
0.020 -0.020 1 18 2 0 0
*
* X/C
0
0.337
1.034
3.417
6.959
11.512
16.911
23.157
30.427
38.575
47.37

56.515
65.666
74.446
82.465
89.349
94.754
100
* XLE1
1.1
* CAMBER ROOT
0.1035
0.2319
0.321
0.4587
0.5358
0.543
0.4572
0.2091
-0.1512
-0.5442
-0.9096
-1.1958
-1.3629
-1.3875
-1.2642
-1.0092
-0.6576
0
* XLE2
1.1
* CAMBER TIP
0.069
0.1546
0.214
0.3058
0.3572
0.362
0.3048
0.1394
-0.1008
-0.3628
-0.6064
-0.7972
-0.9086

-0.925
-0.8428
-0.6728
-0.4384
0
*
*X1 Y1 Z1 CORD1 PANEL 1 UPPER BACK
0.50 0 0.115 0.5
0.86 1.00 0.115 0.5
*NVOR RNCV SPC PDL
20 15 0 0
*AINC1 ANINC2 ITS NAP IQUANT ISYNT NPP
0.39 0.33 1 18 2 0 0
*
* X/C
0
0.337
1.034
3.417
6.959
11.512
16.911
23.157
30.427
38.575
47.37
56.515
65.666
74.446
82.465
89.349
94.754
100
* XLE1
1.1
* CAMBER ROOT
0.1725
0.3865
0.535
0.7645
0.893
0.905
0.762
0.3485

-0.252
-0.907
-1.516
-1.993
-2.2715
-2.3125
-2.107
-1.682
-1.096
0
* XLE2
1.1
* CAMBER TIP
0.138
0.3092
0.428
0.6116
0.7144
0.724
0.6096
0.2788
-0.2016
-0.7256
-1.2128
-1.5944
-1.8172
-1.85
-1.6856
-1.3456
-0.8768
0
*
*X1 Y1 Z1 CORD1 PANEL 2 UPPER BACK
0.86 1.00 0.115 0.5
1.22 2.00 0.115 0.5
*NVOR RNCV SPC PDL
20 15 0 0
*AINC1 ANINC2 ITS NAP IQUANT ISYNT NPP
0.33 0.20 1 18 2 0 0
*
* X/C
0
0.337
1.034

3.417
6.959
11.512
16.911
23.157
30.427
38.575
47.37
56.515
65.666
74.446
82.465
89.349
94.754
100
* XLE1
1.1
* CAMBER ROOT
0.138
0.3092
0.428
0.6116
0.7144
0.724
0.6096
0.2788
-0.2016
-0.7256
-1.2128
-1.5944
-1.8172
-1.85
-1.6856
-1.3456
-0.8768
0
* XLE2
1.1
* CAMBER TIP
0.1035
0.2319
0.321
0.4587
0.5358

0.543
0.4572
0.2091
-0.1512
-0.5442
-0.9096
-1.1958
-1.3629
-1.3875
-1.2642
-1.0092
-0.6576
0
*
*X1 Y1 Z1 CORD1 PANEL 3 UPPER BACK
1.22 2.00 0.115 0.5
1.58 3.00 0.115 0.5
*NVOR RNCV SPC PDL
20 15 0 0
*AINC1 ANINC2 ITS NAP IQUANT ISYNT NPP
0.20 0.00 1 18 2 0 0
*
* X/C
0
0.337
1.034
3.417
6.959
11.512
16.911
23.157
30.427
38.575
47.37
56.515
65.666
74.446
82.465
89.349
94.754
100
* XLE1
1.1
* CAMBER ROOT

0.1035
0.2319
0.321
0.4587
0.5358
0.543
0.4572
0.2091
-0.1512
-0.5442
-0.9096
-1.1958
-1.3629
-1.3875
-1.2642
-1.0092
-0.6576
0
* XLE2
1.1
* CAMBER TIP
0.069
0.1546
0.214
0.3058
0.3572
0.362
0.3048
0.1394
-0.1008
-0.3628
-0.6064
-0.7972
-0.9086
-0.925
-0.8428
-0.6728
-0.4384
0
*
*X1 Y1 Z1 CORD1 PANEL 1 LOWER FRONT
0 0 -0.015 0.5
0.36 1.00 -0.015 0.5
*NVOR RNCV SPC PDL

```
20       15       0        0
*AINC1    ANINC2    ITS      NAP      IQUANT    ISYNT     NPP
0.040     0.020     -1       18       2         0         0
*
* X/C
0
1.239
5.719
11.351
18.681
27.347
36.955
47.473
58.423
65.642
72.561
78.997
84.779
89.754
93.796
96.811
98.753
100
* XLE1
1.1
* CAMBER ROOT
-0.1385
-1.3775
-3.166
-4.336
-5.278
-5.892
-6.023
-5.6675
-5.008
-4.466
-3.8735
-3.253
-2.627
-2.016
-1.437
-0.9055
-0.416
0
```

```
* XLE2
1.1
* CAMBER TIP
-0.1108
-1.102
-2.5328
-3.4688
-4.2224
-4.7136
-4.8184
-4.534
-4.0064
-3.5728
-3.0988
-2.6024
-2.1016
-1.6128
-1.1496
-0.7244
-0.3328
0
*
*X1       Y1        Z1        CORD1   PANEL 2 LOWER FRONT
0.36      1.00      -0.015    0.5
0.72      2.00      -0.015    0.5
*NVOR     RNCV      SPC       PDL
20        15        0         0
*AINC1    ANINC2    ITS       NAP       IQUANT    ISYNT     NPP
0.020     0.020     -1        18        2         0         0
*
* X/C
0
1.239
5.719
11.351
18.681
27.347
36.955
47.473
58.423
65.642
72.561
78.997
84.779
```

89.754
93.796
96.811
98.753
100
* XLE1
1.1
* CAMBER ROOT
-0.1108
-1.102
-2.5328
-3.4688
-4.2224
-4.7136
-4.8184
-4.534
-4.0064
-3.5728
-3.0988
-2.6024
-2.1016
-1.6128
-1.1496
-0.7244
-0.3328
0
* XLE2
1.1
* CAMBER TIP
-0.0831
-0.8265
-1.8996
-2.6016
-3.1668
-3.5352
-3.6138
-3.4005
-3.0048
-2.6796
-2.3241
-1.9518
-1.5762
-1.2096
-0.8622

-0.5433
-0.2496
0
*
*X1 Y1 Z1 CORD1 PANEL 3 LOWER FRONT
0.72 2.00 -0.015 0.5
1.08 3.00 -0.015 0.5
*NVOR RNCV SPC PDL
20 15 0 0
*AINC1 ANINC2 ITS NAP IQUANT ISYNT NPP
0.020 -0.020 -1 18 2 0 0
*
* X/C
0
1.239
5.719
11.351
18.681
27.347
36.955
47.473
58.423
65.642
72.561
78.997
84.779
89.754
93.796
96.811
98.753
100
* XLE1
1.1
* CAMBER ROOT
-0.0831
-0.8265
-1.8996
-2.6016
-3.1668
-3.5352
-3.6138
-3.4005
-3.0048
-2.6796

-2.3241
-1.9518
-1.5762
-1.2096
-0.8622
-0.5433
-0.2496
0
* XLE2
1.1
* CAMBER TIP
-0.0554
-0.551
-1.2664
-1.7344
-2.1112
-2.3568
-2.4092
-2.267
-2.0032
-1.7864
-1.5494
-1.3012
-1.0508
-0.8064
-0.5748
-0.3622
-0.1664
0
*
*X1 Y1 Z1 CORD1 PANEL 1 LOWER BACK
0.50 0 0.085 0.5
0.86 1.00 0.085 0.5
*NVOR RNCV SPC PDL
20 15 0 0
*AINC1 ANINC2 ITS NAP IQUANT ISYNT NPP
0.39 0.33 -1 18 2 0 0
*
* X/C
0
1.239
5.719
11.351
18.681

27.347
36.955
47.473
58.423
65.642
72.561
78.997
84.779
89.754
93.796
96.811
98.753
100
* XLE1
1.1
* CAMBER ROOT
-0.1385
-1.3775
-3.166
-4.336
-5.278
-5.892
-6.023
-5.6675
-5.008
-4.466
-3.8735
-3.253
-2.627
-2.016
-1.437
-0.9055
-0.416
0
* XLE2
1.1
* CAMBER TIP
-0.1108
-1.102
-2.5328
-3.4688
-4.2224
-4.7136
-4.8184

-4.534
-4.0064
-3.5728
-3.0988
-2.6024
-2.1016
-1.6128
-1.1496
-0.7244
-0.3328
0
*
*X1 Y1 Z1 CORD1 PANEL 2 LOWER BACK
0.86 1.00 0.085 0.5
1.22 2.00 0.085 0.5
*NVOR RNCV SPC PDL
20 15 0 0
*AINC1 ANINC2 ITS NAP IQUANT ISYNT NPP
0.33 0.20 -1 18 2 0 0
*
* X/C
0
1.239
5.719
11.351
18.681
27.347
36.955
47.473
58.423
65.642
72.561
78.997
84.779
89.754
93.796
96.811
98.753
100
* XLE1
1.1
* CAMBER ROOT
-0.1108
-1.102

-2.5328
-3.4688
-4.2224
-4.7136
-4.8184
-4.534
-4.0064
-3.5728
-3.0988
-2.6024
-2.1016
-1.6128
-1.1496
-0.7244
-0.3328
0
* XLE2
1.1
* CAMBER TIP
-0.0831
-0.8265
-1.8996
-2.6016
-3.1668
-3.5352
-3.6138
-3.4005
-3.0048
-2.6796
-2.3241
-1.9518
-1.5762
-1.2096
-0.8622
-0.5433
-0.2496
0
*
*X1 Y1 Z1 CORD1 PANEL 3 LOWER BACK
1.22 2.00 0.085 0.5
1.58 3.00 0.085 0.5
*NVOR RNCV SPC PDL
20 15 0 0
*AINC1 ANINC2 ITS NAP IQUANT ISYNT NPP

0.20 0.00 -1 18 2 0 0
*
* X/C
0
1.239
5.719
11.351
18.681
27.347
36.955
47.473
58.423
65.642
72.561
78.997
84.779
89.754
93.796
96.811
98.753
100
* XLE1
1.1
* CAMBER ROOT
-0.0831
-0.8265
-1.8996
-2.6016
-3.1668
-3.5352
-3.6138
-3.4005
-3.0048
-2.6796
-2.3241
-1.9518
-1.5762
-1.2096
-0.8622
-0.5433
-0.2496
0
* XLE2
1.1

```
* CAMBER TIP
-0.0554
-0.551
-1.2664
-1.7344
-2.1112
-2.3568
-2.4092
-2.267
-2.0032
-1.7864
-1.5494
-1.3012
-1.0508
-0.8064
-0.5748
-0.3622
-0.1664
0
*
*X1      Y1       Z1       CORD1   ENDPLATE LOWER
1.08     3.00     0.015    1.0
1.08     3.00     -0.015   1.0
*NVOR    RNCV     SPC      PDL
10       15       0        0
*AINC1   ANINC2   ITS      NAP      IQUANT   ISYNT    NPP
0        0        0        0        2        0        0
*
*X1      Y1       Z1       CORD1   ENDPLATE MIDDLE 1
1.08     3.00     0.085    1.0
1.08     3.00     0.015    1.0
*NVOR    RNCV     SPC      PDL
10       15       0        0
*AINC1   ANINC2   ITS      NAP      IQUANT   ISYNT    NPP
0        0        0        0        2        0        0
*
*X1      Y1       Z1       CORD1   ENDPLATE MIDDLE 2
1.08     3.00     0.115    1.0
1.08     3.00     0.085    1.0
*NVOR    RNCV     SPC      PDL
10       15       0        0
*AINC1   ANINC2   ITS      NAP      IQUANT   ISYNT    NPP
0        0        0        0        2        0        0
*
```

```
*X1       Y1       Z1       CORD1   ENDPLATE UPPER
1.08     3.00     0.485    1.0
1.08     3.00     0.115    1.0
*NVOR    RNCV     SPC      PDL
20       15       0        0
*AINC1   ANINC2   ITS      NAP      IQUANT   ISYNT    NPP
0        0        0        0        2        0        0
*
*NXS     NYS      NZS
0        0        0
*END
```

APPENDIX B

CREATIVE COMMONS COPYRIGHT FOR PIXABAY

Source: https://pixabay.com/service/license-summary/

Content License Summary

Welcome to Pixabay! Pixabay is a vibrant community of authors, artists and creators sharing royalty-free images, video, audio and other media. We refer to this collectively as "Content". By accessing and using Content, or by contributing Content, you agree to comply with our Content License.

At Pixabay, we like to keep things as simple as possible. For this reason, we have created this short summary of our Content License which is available in full here. Please keep in mind that only the full Content License is legally binding.

What are you allowed to do with Content?

Subject to the Prohibited Uses (see below), the Content License allows users to:

✓ Use Content for free

✓ Use Content without having to attribute the author (although giving credit is always appreciated by our community!)

✓ Modify or adapt Content into new works

What are you not allowed to do with Content?

We refer to these as Prohibited Uses which include:

× You cannot sell or distribute Content (either in digital or physical form) on a Standalone basis. Standalone means where no creative effort has been applied to the Content and it remains in substantially the same form as it exists on our website.

× If Content contains any recognisable trademarks, logos or brands, you cannot use that Content for commercial purposes in relation to goods and services. In particular, you cannot print that Content on merchandise or other physical products for sale.

× You cannot use Content in any immoral or illegal way, especially Content which features recognisable people.

× You cannot use Content in a misleading or deceptive way.

Please be aware that certain Content may be subject to additional intellectual property rights (such as copyrights, trademarks, design rights), moral rights, proprietary rights, property rights, privacy rights or similar. It is your responsibility to check whether you require the consent of a third party or a license to use Content.

93

APPENDIX C

CREATIVE COMMONS LICENCE FOR 1990 BENETTON B190

APPENDIX D

CREATIVE COMMONS LICENSE FOR ARROWS SUPERTEX A21

APPENDIX E

CREATIVE COMMONS LICENSE FOR DE TOMASO 505

You are free to:

Share — copy and redistribute the material in any medium or format for any purpose, even commercially.

Adapt — remix, transform, and build upon the material for any purpose, even commercially.

The licensor cannot revoke these freedoms as long as you follow the license terms.

Under the following terms:

Attribution - You must give appropriate credit , provide a link to the license, and indicate if changes were made . You may do so in any reasonable manner, but not in any way that suggests the licensor endorses you or your use.

ShareAlike - If you remix, transform, or build upon the material, you must distribute your contributions under the same license as the original.

No additional restrictions - You may not apply legal terms or technological measures that legally restrict others from doing anything the license permits.

Notices:

You do not have to comply with the license for elements of the material in the public domain or where your use is permitted by an applicable exception or limitation .

No warranties are given. The license may not give you all of the permissions necessary for your intended use. For example, other rights such as publicity, privacy, or moral rights may limit how you use the material.

Source: https://creativecommons.org/licenses/by-sa/2.0/99